September 20, 2021

Functional Analysis of the Expanded Phosphodiesterase Gene Family in *Toxoplasma gondii* Tachyzoites

William J. Moss[1], Caitlyn E. Patterson[1], Alexander K. Jochmans[2], and Kevin M. Brown[1,3]

[1]Department of Microbiology and Immunology, University of Oklahoma Health Sciences Center, Oklahoma City, Oklahoma, USA

[2]Department of Biology, Rogers State University, Claremore, Oklahoma, USA

[3]Address correspondence to Kevin M. Brown, kevin-brown@ouhsc.edu

Running title: Role of Phosphodiesterases in *T. gondii*

Abstract

Toxoplasma motility is both activated and suppressed by 3'-5' cyclic nucleotide signaling. Cyclic GMP (cGMP) signaling through TgPKG activates motility, whereas cyclic AMP (cAMP) signaling through TgPKAc1 inhibits motility. Despite being master regulators of motility, it is unclear how cGMP and cAMP levels are maintained in *Toxoplasma*. Phosphodiesterases (PDEs) are known to inactivate cyclic nucleotides and are highly expanded in the *Toxoplasma* genome. Here we utilized an auxin-inducible degron system to analyze the expression and function of the 18-member TgPDE family in tachyzoites, the virulent life stage of *Toxoplasma*. We detected the expression of 11 of 18 TgPDEs by immunofluorescence microscopy or immunoblotting, confirming prior expression studies. We performed a knockdown screen of the TgPDE family and identified four TgPDEs that contribute to lytic *Toxoplasma* growth (TgPDE1, TgPDE2, TgPDE5, and TgPDE9). Loss of TgPDE1 and TgPDE2 caused severe growth defects, prompting further investigation. TgPDE1 displayed a plasma membrane/cytomembranous distribution, whereas TgPDE2 displayed an endoplasmic reticulum-like distribution. Biochemical analysis of TgPDE1 and TgPDE2 purified from *Toxoplasma* lysates revealed that they are active phosphodiesterases. TgPDE1 was capable of hydrolyzing both cGMP and cAMP, whereas TgPDE2 was cAMP-specific. Interactome studies of TgPDE1 and TgPDE2 indicated that they do not physically interact with each other or other TgPDEs but may be regulated by kinases and proteases. Our studies have identified TgPDE1 and TgPDE2 as central regulators of tachyzoite cyclic nucleotide levels and enable future studies aimed at determining how these enzymes are regulated and cooperate to control *Toxoplasma* motility.

Importance

Apicomplexan parasites require motility to actively infect host cells and cause disease. Cyclic nucleotide signaling governs apicomplexan motility but it is unclear how cyclic nucleotide levels are maintained in these parasites. In search of novel regulators of cyclic nucleotides in the model apicomplexan *Toxoplasma*, we identified and characterized two catalytically active phosphodiesterases, TgPDE1 and TgPDE2, that are important for *Toxoplasma*'s virulent tachyzoite lifecycle. Enzymes that generate, sense, or degrade cyclic nucleotides make attractive targets for therapies aimed at paralyzing and killing apicomplexan parasites.

Introduction

Apicomplexan parasites are obligate-intracellular protozoan parasites that cause a variety of deadly diseases including malaria, cryptosporidiosis, and toxoplasmosis. Several species of *Plasmodium* cause human malaria, such as *P. falciparum* and *P. vivax*, resulting in hundreds of thousands of deaths annually (1). *Cryptosporidium parvum and C. hominis* are the main agents of human cryptosporidiosis, a diarrheal disease that kills tens of thousands of children and infants each year (2). *Toxoplasma gondii* (*Toxoplasma*) infections are less deadly, but are much more widespread. *Toxoplasma* infects and persists within 25-30% of the global human population and causes toxoplasmosis, which can be fatal for immunosuppressed individuals or developing fetuses (3). Although apicomplexan parasites cause distinct diseases in numerous organ systems, lytic parasite growth is the primary source of pathogenesis caused by apicomplexan parasites (4). Therefore, a better understanding of how these parasites progress through their lytic cycles will reveal molecular targets for novel therapeutic interventions.

The apicomplexan asexual lytic cycle occurs in five general steps: attachment to a host cell, invasion, formation of the parasitophorous vacuole (PV), intracellular replication, and egress (5). Attachment comprises interactions between parasite and host surface proteins/glycoproteins. Upon firm attachment, secretion of specialized secretory organelles called micronemes and rhoptries embed a ring-like invasion complex into the host cell plasma membrane that forms a transient portal for parasite entry (6). The parasite glideosome, a surface adhesin-linked actin-myosin motor, provides the locomotive force for invasion and other motile processes (5). During

invasion, the PV is formed from host plasma membrane (stripped of host proteins) and provides an interface between the parasite host for parasite effector export, immune subversion, and nutrient acquisition (7-9). Once inside the PV, parasites undergo asexual replication generating up to several dozens of newly formed parasites (4). To conclude the lytic cycle, parasites secrete pore-forming microneme proteins and upregulate motility to egress from the PV and host cell (10). The parasite lytic cycle directly results in tissue destruction, increased parasite burden, and subsequent inflammation that is the cornerstone of apicomplexan virulence and pathogenesis. Therefore, understanding how parasites modulate motility for lytic growth is critical to understanding how they cause disease.

Apicomplexans have adapted second messenger signaling systems to regulate microneme secretion and motility (11-15). Purine cyclic nucleotides (cGMP and cAMP) and ionic calcium (Ca^{2+}) signaling pathways are central regulators of apicomplexan motility, but there are species-dependent variations in how they operate. In general, external signals will stimulate parasite guanylate cyclase(s) to produce cGMP from GTP (16-26). Accumulation of cGMP in the parasite cytosol will activate protein kinase G (PKG), the only known cGMP effector in apicomplexans (27). Catalytically active PKG is required for microneme secretion and motility by stimulating Ca^{2+} flux, and through an unknown mechanism that cannot be bypassed by exogenous Ca^{2+} (28-34). PKG is thought to stimulate release of Ca^{2+} stores by upregulating inositol 1,4,5-trisphosphate (IP_3) signaling and by phosphorylating ICM1, a multipass membrane protein essential for PKG-dependent calcium mobilization (35). Cytosolic Ca^{2+} activates Ca^{2+}-binding proteins that regulate microneme secretion (e.g. calcium-dependent protein kinases,

vesicle fusion machinery) and motility (e.g. calmodulins) (36-38). The role of cAMP signaling is less conserved in Apicomplexa, where cAMP signaling through protein kinase A catalytic subunit (PKAc) acts in concert with cGMP and Ca^{2+} for *Plasmodium* invasion (13, 39-43), yet PKAc1 inhibits motility following invasion by negatively regulating Ca^{2+} in *Toxoplasma* (44, 45). In either scenario, it is clear that cyclic nucleotide levels must be tightly controlled for timely motility in Apicomplexa.

There is growing evidence for the importance of cyclic nucleotide turnover in apicomplexan parasites. Phosphodiesterases (PDEs) inactivate cyclic nucleotides through hydrolysis (46) and are conserved in Apicomplexa (47). Studies using mammalian PDE inhibitors provided the first experimental evidence for the importance of apicomplexan PDEs. Zaprinast and BIPPO upregulate parasite cGMP-dependent motility, while prolonged treatment is lethal (48). Similarly, 3-isobutyl-1-methylxanthine (IBMX) upregulates parasite cAMP and modulates parasite motility, growth and development but its effects are likely species- and life-stage-dependent (47, 49, 50). At the single gene level, most of what is known about apicomplexan PDEs comes from *Plasmodium* research. *Plasmodium* encodes four PDEs (α/β/γ/δ) that all degrade cGMP, with PDEβ (essential in asexual blood stages) also possessing cAMP hydrolytic activity (13, 51). *Cryptosporidium* also encodes a limited set of PDEs (three) but have yet to be characterized. In contrast, *Toxoplasma* encodes 18 PDEs of unknown functional significance. Recent expression studies indicated that the *Toxoplasma* PDE family consists of life-stage dependent PDEs with diverse subcellular localizations (44, 52, 53). Similar to *Plasmodium* PDEβ (42), *Toxoplasma* PDE8 and PDE9 are dual-specific PDEs, although PDE9 was deemed dispensable for tachyzoite growth (53). It is

currently unclear which PDEs are primarily responsible for cGMP and/or cAMP turnover in *Toxoplasma* or whether they are functionally redundant.

To facilitate the functional analysis of the *Toxoplasma* PDE family, we created conditional knockdown lines for each TgPDE using a mini-auxin-inducible degron (mAID) system (33). Using this system, we assessed the expression and localization of each TgPDE in the virulent tachyzoite life-stage and measured their contributions to lytic growth following conditional knockdown. We determined that TgPDE1 and TgPDE2 were critical for lytic parasite growth and possessed distinct cyclic nucleotide preferences and subcellular distributions. Furthermore, interactome studies of TgPDE1 and TgPDE2 indicated that they may function in unique signaling complexes and receive novel modes of regulation. Taken together, our studies have identified TgPDE1 and TgPDE2 as central regulators of tachyzoite cyclic nucleotide levels and enable future studies aimed at determining how these enzymes are regulated and cooperate to control motility for lytic growth.

Results

Toxoplasma encodes 18 putative PDEs with diverse domain architectures.

There are 18 phosphodiesterases visible in the *Toxoplasma* genome, but their roles in cyclic nucleotide turnover and parasite fitness are largely undetermined. One or more TgPDEs are suspected to be vital to the tachyzoite lytic lifecycle as treatment with human PDE inhibitors, like zaprinast, blocks plaque formation (48) (Fig. S1). Conversely, we noted that the non-selective broad-spectrum human PDE inhibitor IBMX does not inhibit tachyzoite growth at high concentration (0.5 mM), indicating that inhibition of host PDEs does not significantly impact parasite growth and that zaprinast

likely targets an essential TgPDE or subset of TgPDEs (Fig. S1). Furthermore, a genome-wide CRISPR knockout screen indicated that five TgPDEs are potentially important for tachyzoite fitness *in vitro* (phenotype scores <-1) (54). Similarly, *TgPDE1* and *TgPDE2* are refractory to deletion in tachyzoites providing strong indirect evidence for their importance (44). Collectively, these findings compelled us to investigate the function of the TgPDE family in *Toxoplasma*.

Adhering to the TgPDE nomenclature designated by Vo et al. 2020 (53), we analyzed each TgPDE protein sequence for conserved domains using the NCBI Conserved Domain database (55). We determined that TgPDE proteins ranged from 311 aa (TgPDE14) to 3476 aa (TgPDE18) in length with variable domain architectures. Each TgPDE contained a single C-terminal PDEase_I domain (pfam00233), which hydrolyze 3’5’-cyclic nucleotides such as cAMP and cGMP (Fig. 1). TgPDE4 and TgPDE16 contained portions of an ion-transport domain (pfam00520) suggesting they may also regulate, or be regulated by, ion-transport (Fig. 1). TgPDE2 contained a GAF domain (pfam01590) known to bind cyclic nucleotides and modulate PDE activity (56) (Fig. 1). Low confidence non-specific domain fragments (not shown) were also detected for TgPDE7 (transcriptional regulator ICP4, cl33723), TgPDE9 (transcriptional termination factor Rho, cl36163), TgPDE15 (OCRE, cl23757), and TgPDE18 (MAEBL, cl31754; transcriptional termination factor Rho, cl36163; U2 snRNP auxiliary factor, cl36941). Transmembrane domains within TgPDE proteins were predicted using TOPCONS (57). Except for TgPDE2, TgPDE3, and TgPDE14, all other TgPDEs had 2-7 transmembrane domains (Fig. 1), suggesting that most TgPDEs are integral membrane proteins. Therefore, the expanded TgPDE family appears well-suited to

degrade cyclic nucleotides in a variety of subcellular compartments with diverse modes of regulation and secondary functions.

Expression and distribution of TgPDEs in tachyzoites.

To investigate the expression of each TgPDE in tachyzoites, we implemented an auxin-inducible degron system for detection and conditional depletion of mAID-3HA tagged proteins (33). Starting with RH TIR1-3FLAG, which expresses the plant auxin receptor TIR1, we used CRISPR/Cas9 genome editing (58) to tag each *TgPDE* gene with a short homology-flanked *mAID-3HA, HXGPRT* cassette (Fig. 2A) as described (59). Following drug selection and isolation of clones, genomic DNA was harvested for diagnostic PCRs to distinguish untagged clones from mAID-3HA tagged clones. Our primer design allowed integration validation such that PCR1 should only show a 283-335 bp band in untagged wildtype genomic DNA, while PCR2 should only show a 493-534 bp band in TgPDE-mAID-3HA genomic DNA depending on each *TgPDE* gene. Diagnostic PCR revealed that each *TgPDE* was successfully tagged with the *mAID-3HA, HXGPRT* for detection and functional analyses (Fig. 2B).

To determine which TgPDEs are expressed in tachyzoites, we used immunofluorescence (IF) microscopy and immunoblotting to detect the 3HA epitope for each TgPDE-mAID-3HA fusion. TgPDE1, 2, 5, 6, 7, 9, 10, 11, 12, 13, and 18 showed expression in tachyzoites by IF microscopy and/or immunoblotting (Fig. 3). We were unable to detect TgPDE8 by either method, which can be detected with the more sensitive spaghetti monster-HA (smHA) tag in tachyzoites (53). Of the TgPDEs detected by IF microscopy, we observed diverse subcellular distribution patterns reminiscent of plasma membrane (TgPDE1, 2, 7, 10, 13, 18), endoplasmic reticulum (TgPDE2, 11),

mitochondrion (TgPDE5), nucleus (TgPDE6), and apical cap (TgPDE9) (Fig. 3A). Co-staining with markers for each compartment and super-resolution microscopy will be needed to precisely localize each TgPDE going forward. Of the TgPDEs detected by immunoblotting, all could be detected in full-length, but with smaller isoforms also detected for TgPDE2, 7, and 10 indicating that they could be regulated through alternative splicing or proteolysis (Fig. 3B). To determine whether auxin-treatment could deplete the TgPDE-mAID-3HA fusions, parasites were treated with vehicle or 0.5 mM auxin (3-indoleacetic acid; IAA) for 18 h, lysed, and analyzed by SDS-PAGE with immunoblotting for the 3HA epitope. We observed that all detectable TgPDE-mAID-3HA fusions were efficiently depleted following auxin treatment (Fig. 3B). Taken together, we have identified at least 11 TgPDEs that may regulate cyclic nucleotide turnover in tachyzoites and have developed a robust knockdown system for assessing the function of each member of the TgPDE family.

Four TgPDEs contribute to the tachyzoite lytic lifecycle.

To assess the individual contribution of each TgPDE to overall tachyzoite fitness, we performed plaque assays for all 18 TgPDE conditional knockdown mutants. We reasoned that even TgPDEs expressed below the limit of detection may still serve important functions, so they were also included in the screen. Freshly-harvested RH TIR1-FLAG and RH PDE-mAID-3HA tachyzoites were inoculated onto HFF monolayers, treated with 0.5 mM IAA (to deplete mAID-3HA fusions) or vehicle for 8 days, fixed with ethanol, and stained with crystal violet to visualize plaque formation (e.g. macroscopic zones of clearance on host cell monolayers). Since plaque formation requires the completion of several rounds of lytic growth, defects in any step of the lytic cycle will

reduce plaque formation. As previously reported (33, 38), IAA did not affect the ability of RH TIR1-3FLAG to form plaques (Fig. 4). However, we observed that knockdown of four TgPDEs caused significant plaquing defects compared to vehicle treatment (Fig. 4). Loss of TgPDE5 and TgPDE9 reduced plaque area, indicated suboptimal lytic growth (Fig. 4). In contrast, loss of TgPDE1 and TgPDE2 significantly reduced both plaque area and the number of plaques formed (Fig. 4). TgPDE2 had the most profound contribution to tachyzoite growth, reducing plaque area by ~95%. The non-redundant phenotypes associated with separate TgPDE1 and TgPDE2 depletion suggests that they may have unique cyclic nucleotide preferences which would lead to opposing roles in regulating motility for lytic cycle progression.

Biochemical activities of TgPDEs.

To determine the substrate preference of each TgPDE, we first generated recombinant 6HIS-SUMO fusions of TgPDE catalytic domain fragments (6HIS-SUMO-TgPDE^{CAT}) from *E. coli*. This strategy was chosen to facilitate expression, solubility, and purification of non-denatured TgPDE^{CAT} fragments based on the retained activity of 5HIS-PfPDEα^{CAT}, an analogous fragment of a cGMP-specific PDE from *P. falciparum* purified from *E. coli* (47). For *E. coli* expression, TgPDE^{CAT} fragments (Fig. S2A) were cloned from GT1 tachyzoite cDNA libraries or synthesized as dsDNA gene fragments and ligated into pET-*6HIS-SUMO* (60). Similar constructs containing PfPDEα^{CAT} and PfPDEβ^{CAT} or HsGSDMD (human gasdermin D) served as positive and negative controls for PDE activity, respectively. The sequence-verified expression constructs were then transformed into SHuffle T7 *E. coli*, induced with isopropylthio-β-galactoside (IPTG), and 6HIS-SUMO protein fusions were purified from sarkosyl-solubilized

inclusion bodies using immobilized metal affinity chromatography with Ni-NTA gravity flow columns (Fig. S2B). The recombinant protein fractions were analyzed by SDS-PAGE with total protein staining and we determined that each 6HIS-SUMO-TgPDE^{CAT} protein was captured and adequately purified for downstream analysis (Fig. S3). To determine whether the recombinant 6HIS-SUMO-TgPDE^{CAT} proteins possessed PDE activity, we performed PDE-Glo assays using cAMP or cGMP as the relevant substrate (Fig. S4A). Unfortunately, we were unable to reliably detect PDE activity for the 6HIS-SUMO-TgPDE^{CAT} proteins with even 2 h reactions at 37°C (Figure S4B, S4C). These results suggest that generating catalytically-active recombinant TgPDE^{CAT} proteins will require further optimization (detergents, refolding, etc.) or that TgPDEs need to be purified in full-length from *Toxoplasma* to retain activity.

To determine whether endogenously-expressed TgPDEs are active, we focused on the two most critical TgPDEs for tachyzoite growth: TgPDE1 and TgPDE2 (Fig. 4). We used immunoprecipitation (IP) to capture TgPDE1-mAID-3HA and TgPDE2-mAID-3HA from native soluble tachyzoite lysates using anti-HA magnetic chromatography with HA peptide elution (Fig. 5A). IP fractions for total protein, soluble protein, and eluted protein were analyzed by immunoblotting and we observed that TgPDE1 and TgPDE2 were effectively captured (Fig. 5B). We believe the non-denaturing detergents in the native lysis buffer interacted with the transmembrane domains of TgPDE1 and slowed its migration during SDS-PAGE, as has been described for other transmembrane proteins (61, 62). In agreement, the supershifted species of TgPDE1-mAID-3HA was not observed when lysates were prepared without these detergents (Fig. 3B). Due to the nature of the HA peptide elution, and relatively low yield of immunoprecipitated

proteins, we were unable to measure the exact concentrations of captured proteins. Therefore, we performed PDE-Glo assays using equivalent volumes of IP elution fractions with the untagged parental line elution fraction serving as the background threshold for PDE activity. Upon addition of 200 nM cAMP substrate, eluted TgPDE1 and TgPDE2 fractions were clearly capable of hydrolyzing cAMP as compared to the negative control and standards (Figure 5C). When 20 μM cGMP substrate was supplied, only eluted TgPDE1 was able to hydrolyze cGMP (Figure 5D).

To determine if any other TgPDEs were unexpectedly pulled down with TgPDE1-mAID-3HA or TgPDE2-mAID-3HA, we performed similar IP experiments without HA peptide elution and analyzed all captured proteins by liquid chromatography mass spectrometry (LC-MS/MS) (Figure S5A). In this case, RH YFP-AID-3HA served as a control for non-specific protein interactions. IP fractions were first analyzed by total protein staining and immunoblotting (Fig. S5B,C). While the relative abundance of captured protein was low (Fig. S5B), we were able to clearly detect the target proteins by immunoblotting (Fig. S5C). TgPDE1-mAID-3HA and TgPDE2-mAID-3HA both retained hydrolytic activity while immobilized on anti-HA magnetic beads, indicating that native protein complexes were captured (Fig. S5D). Importantly, no other TgPDE co-immunoprecipitated with either TgPDE1 or TgPDE2 in two independent trials (Fig. S5E, Table S4). Furthermore, formaldehyde-crosslinking protein interactions prior to parasite lysis and IP (XL-LC-MS/MS) did not stabilize interactions between TgPDE1 and TgPDE2 or any other TgPDE (Table S5). However, these interactome studies indicate that TgPDE1 and TgPDE2 are potentially regulated by other proteins through protein-protein interactions and/or post-translational modifications. Collectively, our

investigation of the TgPDE family revealed that TgPDE1 is a dual-specific PDE and TgPDE2 is a cAMP-specific PDE that are critical for tachyzoite lytic growth.

Discussion

Recent studies have demonstrated that purine 3'-5' cyclic nucleotides, cGMP and cAMP, are master regulators of lytic lifecycle progression in *Toxoplasma* (12, 15). While prior studies focused on the biosynthesis and effector functions of these signaling molecules, here we focused on an expanded family of PDEs to identify regulators of cyclic nucleotide turnover. Comparative genomics revealed that coccidian apicomplexans encode 8-19 PDE genes, the most out of the four principle apicomplexan groups (gregarina, cryptosporidia, hematozoa, coccidia) (https://www.veupathdb.org/). *Toxoplasma* serves as an tractable model for investigating coccidian PDEs since it encodes 18 representative PDEs. *Toxoplasma* PDEs have a core domain architecture consisting of a C-terminal PDEase_I domain and variable N-terminal features, although mutational analysis will be needed to identify domains necessary for TgPDE function. By tagging each TgPDE gene with a regulatable epitope tag, we were able to detect 11 TgPDEs expressed in tachyzoites with a variety of subcellular distributions. Our conditional knockdown screen of the TgPDE family revealed that four TgPDEs (TgPDE1, 2, 5, 9) independently contribute to tachyzoite growth. From these, TgPDE1 and TgPDE2 emerged as principle regulators of tachyzoite fitness. TgPDE1 and TgPDE2 displayed distinct subcellular localizations, cyclic nucleotide preferences, and interactomes, suggesting opposing roles in cyclic nucleotide regulation in tachyzoites.

Studies of PDE function in many apicomplexans have been hindered by the sheer number of PDEs encoded in their genomes. This is especially true for coccidian apicomplexans like *Toxoplasma* that encode 18 PDE genes (Fig. 1). In contrast, other apicomplexan groups like hematozoa (i.e. malarial parasites and piroplasms) encode only 2-4 PDE genes per species. This discrepancy begs the question: why do coccidian apicomplexans need so many PDEs? We speculate that PDE expansion in coccidia meets the demands of their asexual (acute and chronic) and sexual life-stages, compartmentalized signaling, and serves as a redundancy safeguard for added control. Transcriptome-wide expression studies have indicated a life-stage dependence for the majority of TgPDEs (52). In support, 11 of 18 TgPDEs were recently shown to be expressed in tachyzoites by IFA and immunoblotting (53), which we were able to largely confirm independently here with disparate epitope tags (Fig. 3). Additional studies are needed to determine which TgPDEs control cyclic nucleotide turnover in other life-stages such as bradyzoites, merozoites, gametes, and sporozoites. We and others have also observed distinct subcellular distributions for TgPDEs (44, 53), indicating that they may act on separate pools of cyclic nucleotides for finely-tuned signaling. Previously we showed that cGMP biosynthesis by TgGC and subsequent TgPKG activation occurs at the plasma membrane (21, 33). Therefore, cGMP-TgPDEs positioned at the plasma membrane would be well-positioned to turn off TgPKG signaling following invasion. The localization of cAMP signaling is more complex and less centralized in *Toxoplasma* (4 TgACs, 2 TgPKArs, 3 TgPKAcs) (21, 44, 45, 50, 63), which may require compartmentalized TgPDEs to inactivate cAMP signaling for egress or development. Overall, it appears beneficial for *Toxoplasma* to have life-stage-

dependent PDEs distributed throughout the cell to prevent or inactivate unwanted cyclic nucleotide signaling.

Despite expressing at least 11 TgPDEs in tachyzoites, we were able to identify several TgPDEs that individually contribute to tachyzoite fitness (Fig. 4). Conditional depletion of TgPDE5 and TgPDE9 modestly reduced the size of plaques formed on HFF monolayers, indicating that they partially contribute to tachyzoite fitness. TgPDE9 was previously determined to be capable of degrading cAMP and cGMP, but was deemed dispensable by knockout in tachyzoites (53). Given the time it takes to generate and maintain knockouts, compensatory suppressor mutations could emerge and mask knockout phenotypes. Since TgPDE8 has the same localization and substrate preference as TgPDE9 (53), upregulation of TgPDE8 could feasibly suppress phenotypes associated with Δ*Tgpde9*. The speed of TgPDE9-mAID-3HA knockdown is unlikely to allow for suppressors, revealing TgPDE9's true contribution to tachyzoite fitness. With loss of TgPDE1, we observed a slight reduction in plaque numbers and the plaques that did form were substantially smaller compared to vehicle treatment. The reduction in plaque numbers indicates that TgPDE1 is essential in a subset of parasites within a population of knockdown mutants. TgPDE2 depletion elicited the most severe plaquing defects, reducing plaque size by ~95%. These data indicate that TgPDE1 and TgPDE2 are indispensable and non-redundant for tachyzoite fitness, which supports the hypothesis that TgPDE1 and TgPDE2 are refractory to deletion (44, 54).

To understand how TgPDE1 and TgPDE2 contribute to tachyzoite fitness, we first tested whether either had phosphodiesterase activity. Attempts to generate highly-active recombinant TgPDE catalytic domain fragments were unsuccessful (Fig. S2-4).

We suspect that the recombinant proteins were not adequately refolded following solubilization of inclusion body preparations and will require further optimization. It is also possible that some TgPDEs are simply catalytically inactive or hydrolyze unknown substrates. As an alternative approach, we performed activity assays on tagged TgPDEs immunoprecipitated from *Toxoplasma* lysates (Fig. 5). TgPDE1 was capable of degrading cGMP and cAMP, while TgPDE2 was cAMP-specific. It is reasonable for TgPDE1 and TgPDE2 to have different substrate preferences since they are both required for tachyzoite fitness and likely serve non-redundant roles. Our data suggests that TgPDE2 is primarily responsible for cAMP degradation in tachyzoites. Therefore, we speculate that TgPDE1 is primarily responsible for cGMP turnover in tachyzoites, with minor contributions from TgPDE8 and TgPDE9 that are also dual-specific PDEs (53), and possibly TgPDE5. It is not known whether dual-specific PDEs act selectively in *Toxoplasma*, but may be important given the mutually exclusive nature of cGMP and cAMP signaling in *Toxoplasma* (12, 15). A combinatorial knockout/knockdown approach is needed to directly address functional redundancy within the TgPDE family.

To ensure that the phosphodiesterase activities we observed for TgPDE1 and TgPDE2 were not artifacts of unexpected interactions with other TgPDEs, we analyzed immunoprecipitated TgPDE1 and TgPDE2 fractions with and without chemical cross-linking by LC-MS/MS (Fig. S5, Table S4, 5). No other TgPDEs co-immunoprecipitated with TgPDE1 or TgPDE2, indicating that TgPDE1 and TgPDE2 were solely responsible for the cyclic nucleotide degradation observed *ex vivo*. However, we did detect unique interactors for TgPDE1 and TgPDE2 that may regulate their activities through proteolysis, localization, or phosphorylation. Identifying domains and modifications that

control TgPDE1 and TgPDE2 activity is critical to understand the mechanisms by which they regulate cyclic nucleotide turnover for lytic growth.

Altogether, our investigation of the 18-member TgPDE family revealed that TgPDE1 and TgPDE2 are the primary phosphodiesterases in *Toxoplasma* tachyzoites. We determined that TgPDE1 is a dual-specific PDE but we hypothesize that it primarily degrades cGMP in *Toxoplasma*. To our knowledge, this work also designates TgPDE2 as the only known cAMP-specific PDE in Apicomplexa. We propose a two-part working model in which 1) TgPDE1 is activated following *Toxoplasma* invasion to turn off cGMP-stimulated motility for replication and 2) TgPDE2 is activated following *Toxoplasma* replication to turn off cAMP-signaling, which inhibits motility, for egress and cell-to-cell transmission. This work enables future studies aimed at determining how TgPDE1 and TgPDE2 are regulated and cooperate to control cyclic nucleotide turnover and lytic growth. Furthermore, due to their conservation, TgPDE1 and TgPDE2 will serve as models for coccidian dual-specific and cAMP-specific PDEs, respectively.

Materials and Methods

Parasite and host cell culture. *T. gondii* tachyzoites were maintained in human foreskin fibroblasts (HFF) monolayers at 37°C, 5% CO_2 in D10 medium: Dulbecco's Modified Eagle's Medium (Gibco) supplemented with 10% fetal bovine serum (Gibco), 10 mM glutamine (Gibco) and 10 µg/ml gentamicin (Gibco). Cell lines were routinely assessed for *Mycoplasma* contamination by PCR using a Myco-Sniff Mycoplasma PCR Detection Kit (MP Biomedicals). All parasite lines used and generated in this study are listed in Table S1.

Antibodies. Mouse anti-HA.11 (Clone 16B12) and Mouse anti-HIS tag (Clone J099B12) were purchased from BioLegend. Rat anti-HA (Clone 3F10) was purchased from Roche. Rabbit anti-TgSAG1 antisera was provided by John Boothroyd, Ph.D. (Stanford University). Goat secondary antibodies conjugated to infrared (IR) dyes and Alexa Fluor dyes were purchased from LI-COR and Invitrogen, respectively.

Plasmids. All plasmids generated in this study were created by Q5 Site-directed Mutagenesis (New England Biolabs) of existing plasmids or HiFi Gibson Assembly (New England Biolabs) of linear dsDNA fragments. Plasmid sequences were confirmed by Sanger sequencing (Genewiz) and mapped using SnapGene v5.2.4 (GSL Biotech). All plasmids used in this study are listed in Table S2.

Primers and PCR. All synthetic ssDNA and dsDNA oligonucleotides were synthesized by Integrated DNA Technologies and are listed in Table S3. Protoscript II Reverse Transcriptase (New England Biolabs) was used to make cDNA PCR templates from parasite RNA (*Toxoplasma* GT1; *Plasmodium falciparum* NF54) extracted with a Monarch Total RNA Miniprep Kit (New England Biolabs). Genomic DNA (*Toxoplasma* RH derivatives) was extracted for PCR using a Monarch Genomic DNA Purification Kit (New England Biolabs). Q5 Polymerase (New England Biolabs) was used for cloning and tagging amplicon PCRs. Taq polymerase (New England Biolabs) was used for diagnostic PCRs.

Sequence analysis. Annotated genomic, transcript, and protein sequences for each TgPDE from Type I reference strain GT1 were downloaded from https://www.toxodb.org/. Transmembrane domains within TgPDE protein sequences were predicted using TOPCONS, a consensus of OCTOPUS, PHILIUS, PolyPhobius,

426 SCAMPI, and SPOCTOPUS algorithms (57). Protein domains and features were
427 predicted using the NCBI conserved domain search against the CDD v3.19 – 58235
428 PSSMs database with an Expect Value threshold of 0.01 (55). The predicted
429 transmembrane domains and features were drawn to scale (primary aa length) using
430 Adobe Illustrator (Adobe, Inc.).

431 **Generation of TgPDE-mAID-3HA conditional knockdown mutants.** RH TIR1-3FLAG
432 tachyzoites were used for tagging TgPDEs with mAID-3HA as described (59). To tag
433 each gene of interest (GOI), a p*SAG1*:*Cas9-GFP*, *U6*:*sgGOI 3' UTR* plasmid (2-5 µg)
434 was co-transfected with a corresponding 40 bp homology arm-flanked *mAID-3HA*,
435 *HXGPRT* amplicon (2-5 µg) into $1x10^6$ RH TIR1-3FLAG tachyzoites in P3 buffer using a
436 4D-nucleofector (Lonza) with pulse code FI-158. Transfected parasites were selected
437 with 25 µg/ml mycophenolic acid (Alfa Aesar) and 50 µg/ml xanthine (Alfa Aesar) in D10
438 medium. Following drug selection, clones were isolated by limiting dilution and epitope
439 tags were confirmed by diagnostic PCR of genomic DNA.

440 **Knockdown of TgPDE-mAID-3HA protein fusions.** Knockdowns were performed as
441 described (59). RH TIR1-3FLAG or RH TgPDE-mAID-3HA tachyzoites cultivated in
442 HFFs in D10 medium were treated with 0.5 mM 3-indoleacetic acid (auxin; IAA) (Sigma
443 Aldrich) prepared in 100% ethanol (Pharmco) or vehicle alone (0.0789% w/v ethanol
444 final concentration) and incubated at 37°C, 5% CO_2 prior to protein detection and/or
445 phenotypic analysis.

446 **Indirect immunofluorescence assay.** Tachyzoite-infected HFF monolayers grown on
447 12 mm #1 glass coverslips (Electron Microscopy Sciences) were fixed with 4%
448 formaldehyde (Polyscience), permeabilized with 0.1% Triton X-100 (MP Biomedicals),

blocked with 10% Normal Goat Serum (Gibco) in phosphate-buffered saline (PBS), labeled with 1:1000 mouse anti-HA, and then washed three times with PBS. Antibody-labeled proteins were fluorescently labeled with 1:2000 goat anti-mouse IgG-AF488, washed five times with PBS, rinsed with water, and mounted on 25x75x1 mm Superfrost Plus glass slides (VWR) with Prolong Gold (Invitrogen). Wide-field images were captured and analyzed with a 100x oil objective on an Axioskop 2 MOT Plus wide-field fluorescence microscope (Carl Zeiss, Inc.) running AxioVision LE64 software (Carl Zeiss, Inc.).

SDS-PAGE and immunoblotting. For routine detection of proteins, tachyzoite pellets were lysed in an equal volume of 2x Laemmli buffer (64) containing 20 mM dithiothreitol (DTT) (Thermo Fisher Scientific). All other protein samples were mixed 4:1 with 5x Laemmli buffer containing 50 mM DTT. Proteins were separated on 4-20% TGX polyacrylamide gels (Bio-Rad) or 4-20% TGX Stain-Free polyacrylamide gels (Bio-Rad) by SDS-PAGE. Total protein in polyacrylamide gels was detected using a ChemiDoc MP Imaging System (Bio-Rad) using Stain-Free (Bio-Rad) or Oriole (Bio-Rad) stains, as indicated in the figure legends. For immunoblotting, proteins separated by SDS-PAGE in polyacrylamide gels were wet-blotted onto nitrocellulose membranes. The membranes were rinsed with PBS containing 0.1% Tween-20 (PBS-T), and then blocked with PBS-T containing 5% (w/v) fat-free powered milk (blocking buffer). Membranes were probed with primary antibodies diluted in blocking buffer, then washed three times with PBS-T. The membranes were then incubated in the dark with goat IR-dye secondary antibodies (LI-COR) diluted in blocking buffer with mixing, then washed

five times with PBS-T. Membranes were imaged on a ChemiDoc MP Imaging System. Gels and membrane blots were analyzed using Image Lab software (Bio-Rad).

Plaque assays. Freshly-egressed tachyzoites (RH TIR1-3FLAG and RH PDE-mAID-3HA lines) were harvested, counted on a hemocytometer, and inoculated (200 parasites/ well) onto confluent HFF monolayers growing in 6-well plates containing D10 medium. To determine the effect of human phosphodiesterase inhibitors on *Toxoplasma* fitness, wells were treated with 0.5 mM 3-isobutyl-1-methylxanthine (IBMX) (MP Biomedicals) prepared in 100% DMSO (Sigma Aldrich), 0.5 mM zaprinast (Tocris) prepared in 100% DMSO or vehicle 0.1% (v/v) DMSO. To determine the effect of conditional knockdown of a TgPDE on *Toxoplasma* fitness, wells were treated with 0.5 mM IAA or 0.0789% w/v ethanol (vehicle). In both experiments, plates were left undisturbed for 8 days in a 37°C, 5% CO_2 incubator. Plaque formation was assessed by counting zones of clearance on EtOH-fixed, crystal violet-stained HFF monolayers. Each stained plate was scanned with high-definition digital scanner (Epson) to obtain representative images and for plaque area analysis. For plaque area measurements, the 10 centermost plaques from the representative wells shown were analyzed using ImageJ to define the plaque area in square pixels (pix^2).

Immunoprecipitation of TgPDE1 and TgPDE2 for activity assays. Freshly-egressed tachyzoites (RH TIR1-3FLAG, RH PDE1-mAID-3HA, and RH PDE2-mAID-3HA) from HFF T150 cultures were scraped, syringe-lysed three times with a 25-ga needle to liberate remaining intracellular parasites, and pelleted (800 x *g*, 4°C, 10 min). Pellets were washed with 30 ml cold PBS and counted on a hemocytometer, then pelleted again. Pellets were washed once more with 1 ml cold PBS, transferred to 2 ml tubes,

then pelleted again. Pellets containing ~ $1x10^8$ parasites were resuspended in 1 ml native lysis buffer (NLB) containing 10 mM K_2HPO_4, 150 mM NaCl, 5 mM EDTA, 5 mM EGTA, pH 7.4, 0.2% sodium deoxycholate, 1% Triton X-100, and 1X protease inhibitor cocktail with EDTA (Pierce), then incubated on ice for 30 minutes with mixing as described (53). Lysates were centrifuged at 14500 x *g*, 4°C, 20 min to remove insoluble material. The soluble supernatant was added to NLB-washed anti-HA magnetic beads (Pierce, 25 µl slurry per IP), and mixed at 4°C for 2 h. A Dynamag (Invitrogen) stand was used to separate beads from supernatant following IP, washing, and elution steps. The beads were washed once with 1 ml NLB, twice with 1 ml PDE storage buffer (40 mM Tris-HCl, 150 mM NaCl, pH 7.5) containing 0.05% Tween-20, and once with 0.2 ml PDE storage buffer. Immunoprecipitated proteins were eluted from beads with 0.2 ml PDE storage buffer containing 1 mg/ml HA-peptide (Thermo Fisher Scientific) with mixing at 37°C for 30 minutes. Bead-free elution fractions and other IP fractions were stored at -80°C until use.

Immunoprecipitation of TgPDE1 and TgPDE2 for LC-MS/MS protein identification. Freshly-egressed tachyzoites (RH YFP-AID-3HA, RH PDE1-mAID-3HA, and RH PDE2-mAID-3HA) from HFF T150 cultures were scraped, syringe-lysed three times with a 25-ga needle to liberate remaining intracellular parasites, and pelleted (800 x *g,* 4°C, 10 min). Pellets were washed with 30 ml cold PBS, counted on a hemocytometer, then pelleted again. For crosslinked IP, parasite pellets were resuspended in cold 6 ml PBS containing 1% formaldehyde (Polyscience) and incubated for 10 min. Following crosslinking, parasites were pelleted and resuspended in 6 ml PBS containing 125 mM glycine for 5 min to quench residual formaldehyde, then pelleted again. Fixed parasite

517 pellets were then resuspended in 30 ml cold PBS. The non-crosslinked and crosslinked
518 parasite suspensions were pelleted and resuspended in 6 ml NLB, syringe disrupted
519 three times with a 25-ga needle, and then spun at 3200 x *g*, 4°C, 50 min to remove
520 insoluble material. The 6 ml soluble lysate fractions were precleared with NLB-washed
521 anti-c-Myc magnetic beads (Pierce, 50 µl slurry per IP) with mixing for 2 h at 4°C. The
522 anti-c-Myc beads were removed by centrifugation (500 x *g*, 4°C, 10 min), and the
523 precleared soluble lysates were incubated with pre-washed anti-HA magnetic beads
524 (Pierce, 50 µl slurry per IP) overnight at 4°C with mixing. The anti-HA magnetic beads
525 were centrifuged (500 x *g*, 4°C, 10 min) and transferred to 1.5 ml tubes for washing
526 using a Dynamag stand. The beads were washed five times with 1 ml NLB and three
527 times with 1 ml PBS. Dry beads and other IP fractions were stored at -80°C until use.
528 Dry beads containing captured proteins were shipped on dry ice to the Proteomics &
529 Metabolomics Facility at the Center for Biotechnology/University of Nebraska – Lincoln
530 for liquid chromatography with tandem mass spectrometry (LC-MS/MS) protein
531 identification. Specific LC-MS/MS analysis parameters are listed in Table S4 (native IP)
532 and S5 (crosslinked IP), respectively.
533 **Expression and purification of 6HIS-SUMO-TgPDE^{CAT} proteins.** SHuffle T7
534 Competent *E. coli* (New England Biolabs) were transformed with pET-*6HIS-SUMO-*
535 *"Protein"* plasmids containing *TgPDE1-18*^{CAT}, *PfPDEα*^{CAT}, *PfPDEβ*^{CAT}, or *HsGSDMD*
536 fusions (listed in Table S2). Transformed *E. coli* starter cultures were grown overnight at
537 30°C in 50 ml Terrific Broth (TB) (Fisher Scientific) containing 50 µg/ml kanamycin with
538 shaking. The cultures were split 1:5 in 250 ml TB containing kanamycin and grown at
539 30°C until reaching an OD_{600} between 0.6 and 0.8. The cultures were induced with 1

mM isopropylthio-β-galactoside (IPTG) (Life Technologies) and grown for 4 h at 30°C. The cells were centrifuged (12000 x *g*, 4°C, 20 min) and the cell pellets were stored at -20°C overnight. The frozen pellets were resuspended in 25 ml cold homogenization buffer: PBS pH 7.4 containing 10 µl/ml Halt Protease Inhibitor Cocktail EDTA-free (Thermo Fisher Scientific) and 2 µl/ml benzonase (Sigma Aldrich). *E. coli* were homogenized using an Emusiflex-C5 (Avestin) with 6 cycles at 20,000 psi. The resulting homogenates were centrifuged (12000 x *g*, 4°C, 20 min) and the insoluble inclusion body fraction was collected (fraction determined to contain recombinant proteins) and solubilized in 4 ml PBS containing 10% (w/v) sarkosyl (MP Biomedicals) with rocking overnight at 4°C. The samples were diluted 1:10 in 40 ml PBS and insoluble material was removed by centrifugation (12000 x *g*, 4°C, 20 min). The soluble supernatants were added to 2 ml pre-equilibrated Ni-NTA slurry (Fisher Scientific), incubated for ~5 h with mixing, then loaded onto to a 10 ml gravity column (Thermo Fisher Scientific) for washing and elution. The resins were washed twice with 40 ml recombinant wash buffer (40 mM Tris-HCl, pH 7.5, and 5 mM imidazole). The recombinant 6HIS-SUMO protein fusions were eluted with 3 ml recombinant elution buffer (40 mM Tris-HCl, pH 7.5, and 250 mM imidazole) and concentrated to 500 µl using Amicon Ultra 10 kDa Spin Columns (Millipore Sigma). The concentrated solutions underwent two buffer exchanges with 500 µl 40 mM Tris-HCl in 0.5 ml Amicon Ultra 10 kDa Spin Columns to reduce the imidazole concentration from 250 mM to ~ 2.5 mM. The partially-purified recombinant proteins were analyzed for purity and identity by SDS-PAGE and immunoblotting with mouse anti-HIS tag, respectively. Protein concentrations were determined using the Rapid Gold BCA Protein Assay kit (Pierce) measured with a

563 Cytation 5 plate imager running Gen5 software (BioTek Instruments). The recombinant
564 proteins were aliquoted and stored at -80°C until use.
565 **Phosphodiesterase activity assays.** To assess the substrate specificity of TgPDEs,
566 recombinant TgPDEs or immunoprecipitated TgPDEs were assayed using the PDE-Glo
567 Phosphodiesterase Assay kit (Promega) according to the manufacturer's instructions
568 with a few modifications. In brief, cyclic nucleotides were diluted in Reaction Buffer (40
569 mM Tris-HCl pH 7.5, 50 mM $MgCl_2$, 0.5 mg/ml BSA). On ice, 10 µl cAMP (2 or 0.2 µM)
570 or cGMP (20 µM) were combined with 10 µl (1 µg) of purified recombinant 6HIS-SUMO-
571 PDE^{CAT} protein or 10 µl immunoprecipitated eluate in triplicate to a 96-well non-skirted
572 natural PCR plate (Midwest Scientific). Cyclic nucleotide standards were diluted further
573 in Reaction Buffer, then 10 µl of standards were combined with 10 µl PDE storage
574 buffer in triplicate in the same plate. To initiate the phosphodiesterase reaction, the
575 plates were sealed and incubated at 37°C for 2 h in a T100 Thermal Cycler (Bio-Rad).
576 After incubation, 10 µl of the phosphodiesterase reaction was added to a 96-well half
577 area flat bottom white polystyrene plate (Greiner) containing 5 µl Termination Buffer.
578 Five µl of Detection Buffer was added to each reaction, covered with parafilm, then
579 incubated at room temperature for 20 min. After incubation, 20 µl Kinase-Glo was added
580 to the reactions, covered with parafilm and foil, and incubated at room temperature for
581 10 min. The resulting luminescence was quantified using a Cytation 5 plate imager
582 running Gen5 software.
583 **Statistical analysis.** Data was graphed and analyzed for statistical significance using
584 GraphPad Prism v 9 (GraphPad Software) using a two-tailed Student's T test for
585 pairwise comparisons of normally distributed data. Error bars represent the standard

deviation or standard error of the mean as indicated in the figure legends. Differences between means were considered statistically significant when P was < 0.05 and designated with one or more asterisks above the graphed data. Non-significant differences between means ($P > 0.05$) were labeled with “ns” in the figures.

Acknowledgements

We thank Sophie Alvarez, Ph.D. and Michael Naldrett, Ph.D. at the Proteomics & Metabolomics Facility at the Center for Biotechnology/University of Nebraska – Lincoln for LC-MS/MS analysis. We thank John Boothroyd, Ph.D. (Stanford University) and the *Toxoplasma* community for antibodies and other key reagents used in this study. We thank Josh Beck, Ph.D. (Iowa State University) for *Plasmodium falciparum* NF54 lysates. Special thanks to L. David Sibley, Ph.D. (Washington University in St. Louis) for professional guidance and support during the developmental stages of this project. This research was supported in part by National Institutes of Health NIAID grant # K22AI144035 to KMB.

References

1. Feachem RGA, Chen I, Akbari O, Bertozzi-Villa A, Bhatt S, Binka F, Boni MF, Buckee C, Dieleman J, Dondorp A, Eapen A, Sekhri Feachem N, Filler S, Gething P, Gosling R, Haakenstad A, Harvard K, Hatefi A, Jamison D, Jones KE, Karema C, Kamwi RN, Lal A, Larson E, Lees M, Lobo NF, Micah AE, Moonen B, Newby G, Ning X, Pate M, Quinones M, Roh M, Rolfe B, Shanks D, Singh B, Staley K, Tulloch J, Wegbreit J, Woo HJ, Mpanju-Shumbusho W. 2019. Malaria eradication within a generation: ambitious, achievable, and necessary. Lancet 394:1056-1112.
2. Guerin A, Striepen B. 2020. The Biology of the Intestinal Intracellular Parasite Cryptosporidium. Cell Host Microbe 28:509-515.
3. Matta SK, Rinkenberger N, Dunay IR, Sibley LD. 2021. Toxoplasma gondii infection and its implications within the central nervous system. Nat Rev Microbiol 19:467-480.
4. White MW, Suvorova ES. 2018. Apicomplexa Cell Cycles: Something Old, Borrowed, Lost, and New. Trends Parasitol 34:759-771.
5. Frenal K, Dubremetz JF, Lebrun M, Soldati-Favre D. 2017. Gliding motility powers invasion and egress in Apicomplexa. Nat Rev Microbiol 15:645-660.
6. Shen B, Sibley LD. 2012. The moving junction, a key portal to host cell invasion by apicomplexan parasites. Curr Opin Microbiol 15:449-55.
7. Clough B, Frickel EM. 2017. The Toxoplasma Parasitophorous Vacuole: An Evolving Host-Parasite Frontier. Trends Parasitol 33:473-488.
8. Matz JM, Beck JR, Blackman MJ. 2020. The parasitophorous vacuole of the blood-stage malaria parasite. Nat Rev Microbiol 18:379-391.
9. Garten M, Beck JR. 2021. Structured to conquer: transport across the Plasmodium parasitophorous vacuole. Curr Opin Microbiol 63:181-188.
10. Guerra AJ, Carruthers VB. 2017. Structural Features of Apicomplexan Pore-Forming Proteins and Their Roles in Parasite Cell Traversal and Egress. Toxins (Basel) 9.
11. Lourido S, Moreno SN. 2015. The calcium signaling toolkit of the Apicomplexan parasites Toxoplasma gondii and Plasmodium spp. Cell Calcium 57:186-93.
12. Bullen HE, Bisio H, Soldati-Favre D. 2019. The triumvirate of signaling molecules controlling Toxoplasma microneme exocytosis: Cyclic GMP, calcium, and phosphatidic acid. PLoS Pathog 15:e1007670.
13. Perrin AJ, Patel A, Flueck C, Blackman MJ, Baker DA. 2020. cAMP signalling and its role in host cell invasion by malaria parasites. Curr Opin Microbiol 58:69-74.
14. Brochet M, Balestra AC, Brusini L. 2021. cGMP homeostasis in malaria parasites-The key to perceiving and integrating environmental changes during transmission to the mosquito. Mol Microbiol 115:829-838.
15. Uboldi AD, Wilde ML, Bader SM, Tonkin CJ. 2021. Environmental sensing and regulation of motility in Toxoplasma. Mol Microbiol 115:916-929.
16. Carucci DJ, Witney AA, Muhia DK, Warhurst DC, Schaap P, Meima M, Li JL, Taylor MC, Kelly JM, Baker DA. 2000. Guanylyl cyclase activity associated with

putative bifunctional integral membrane proteins in Plasmodium falciparum. J Biol Chem 275:22147-56.
17. Muhia DK, Swales CA, Deng W, Kelly JM, Baker DA. 2001. The gametocyte-activating factor xanthurenic acid stimulates an increase in membrane-associated guanylyl cyclase activity in the human malaria parasite Plasmodium falciparum. Mol Microbiol 42:553-60.
18. Hirai M, Arai M, Kawai S, Matsuoka H. 2006. PbGCbeta is essential for Plasmodium ookinete motility to invade midgut cell and for successful completion of parasite life cycle in mosquitoes. J Biochem 140:747-57.
19. Moon RW, Taylor CJ, Bex C, Schepers R, Goulding D, Janse CJ, Waters AP, Baker DA, Billker O. 2009. A cyclic GMP signalling module that regulates gliding motility in a malaria parasite. PLoS Pathog 5:e1000599.
20. Gao H, Yang Z, Wang X, Qian P, Hong R, Chen X, Su XZ, Cui H, Yuan J. 2018. ISP1-Anchored Polarization of GCbeta/CDC50A Complex Initiates Malaria Ookinete Gliding Motility. Curr Biol 28:2763-2776.e6.
21. Brown KM, Sibley LD. 2018. Essential cGMP Signaling in Toxoplasma Is Initiated by a Hybrid P-Type ATPase-Guanylate Cyclase. Cell Host Microbe 24:804-816 e6.
22. Bisio H, Lunghi M, Brochet M, Soldati-Favre D. 2019. Phosphatidic acid governs natural egress in Toxoplasma gondii via a guanylate cyclase receptor platform. Nat Microbiol 4:420-428.
23. Yang L, Uboldi AD, Seizova S, Wilde ML, Coffey MJ, Katris NJ, Yamaryo-Botte Y, Kocan M, Bathgate RAD, Stewart RJ, McConville MJ, Thompson PE, Botte CY, Tonkin CJ. 2019. An apically located hybrid guanylate cyclase-ATPase is critical for the initiation of Ca(2+) signaling and motility in Toxoplasma gondii. J Biol Chem 294:8959-8972.
24. Gunay-Esiyok O, Scheib U, Noll M, Gupta N. 2019. An unusual and vital protein with guanylate cyclase and P4-ATPase domains in a pathogenic protist. Life Sci Alliance 2.
25. Nofal SD, Patel A, Blackman MJ, Flueck C, Baker DA. 2021. Plasmodium falciparum Guanylyl Cyclase-Alpha and the Activity of Its Appended P4-ATPase Domain Are Essential for cGMP Synthesis and Blood-Stage Egress. mBio 12.
26. Jiang Y, Wei J, Cui H, Liu C, Zhi Y, Jiang Z, Li Z, Li S, Yang Z, Wang X, Qian P, Zhang C, Zhong C, Su XZ, Yuan J. 2020. An intracellular membrane protein GEP1 regulates xanthurenic acid induced gametogenesis of malaria parasites. Nat Commun 11:1764.
27. Rotella D, Siekierka J, Bhanot P. 2020. Plasmodium falciparum cGMP-Dependent Protein Kinase - A Novel Chemotherapeutic Target. Front Microbiol 11:610408.
28. Billker O, Lourido S, Sibley LD. 2009. Calcium-dependent signaling and kinases in apicomplexan parasites. Cell Host Microbe 5:612-22.
29. Lourido S, Tang K, Sibley LD. 2012. Distinct signalling pathways control Toxoplasma egress and host-cell invasion. EMBO J 31:4524-34.
30. Collins CR, Hackett F, Strath M, Penzo M, Withers-Martinez C, Baker DA, Blackman MJ. 2013. Malaria parasite cGMP-dependent protein kinase regulates

blood stage merozoite secretory organelle discharge and egress. PLoS Pathog 9:e1003344.

31. Brown KM, Lourido S, Sibley LD. 2016. Serum Albumin Stimulates Protein Kinase G-dependent Microneme Secretion in Toxoplasma gondii. J Biol Chem 291:9554-65.

32. Sidik SM, Hortua Triana MA, Paul AS, El Bakkouri M, Hackett CG, Tran F, Westwood NJ, Hui R, Zuercher WJ, Duraisingh MT, Moreno SN, Lourido S. 2016. Using a Genetically Encoded Sensor to Identify Inhibitors of Toxoplasma gondii Ca2+ Signaling. J Biol Chem 291:9566-80.

33. Brown KM, Long S, Sibley LD. 2017. Plasma Membrane Association by N-Acylation Governs PKG Function in Toxoplasma gondii. MBio 8.

34. Fang H, Gomes AR, Klages N, Pino P, Maco B, Walker EM, Zenonos ZA, Angrisano F, Baum J, Doerig C, Baker DA, Billker O, Brochet M. 2018. Epistasis studies reveal redundancy among calcium-dependent protein kinases in motility and invasion of malaria parasites. Nat Commun 9:4248.

35. Balestra AC, Koussis K, Klages N, Howell SA, Flynn HR, Bantscheff M, Pasquarello C, Perrin AJ, Brusini L, Arboit P, Sanz O, Castano LP, Withers-Martinez C, Hainard A, Ghidelli-Disse S, Snijders AP, Baker DA, Blackman MJ, Brochet M. 2021. Ca(2+) signals critical for egress and gametogenesis in malaria parasites depend on a multipass membrane protein that interacts with PKG. Sci Adv 7.

36. Lourido S, Shuman J, Zhang C, Shokat KM, Hui R, Sibley LD. 2010. Calcium-dependent protein kinase 1 is an essential regulator of exocytosis in Toxoplasma. Nature 465:359-62.

37. Farrell A, Thirugnanam S, Lorestani A, Dvorin JD, Eidell KP, Ferguson DJ, Anderson-White BR, Duraisingh MT, Marth GT, Gubbels MJ. 2012. A DOC2 protein identified by mutational profiling is essential for apicomplexan parasite exocytosis. Science 335:218-21.

38. Long S, Brown KM, Drewry LL, Anthony B, Phan IQH, Sibley LD. 2017. Calmodulin-like proteins localized to the conoid regulate motility and cell invasion by Toxoplasma gondii. PLoS Pathog 13:e1006379.

39. Ono T, Cabrita-Santos L, Leitao R, Bettiol E, Purcell LA, Diaz-Pulido O, Andrews LB, Tadakuma T, Bhanot P, Mota MM, Rodriguez A. 2008. Adenylyl cyclase alpha and cAMP signaling mediate Plasmodium sporozoite apical regulated exocytosis and hepatocyte infection. PLoS Pathog 4:e1000008.

40. Dawn A, Singh S, More KR, Siddiqui FA, Pachikara N, Ramdani G, Langsley G, Chitnis CE. 2014. The central role of cAMP in regulating Plasmodium falciparum merozoite invasion of human erythrocytes. PLoS Pathog 10:e1004520.

41. Furuyama W, Enomoto M, Mossaad E, Kawai S, Mikoshiba K, Kawazu S. 2014. An interplay between 2 signaling pathways: melatonin-cAMP and IP3-Ca2+ signaling pathways control intraerythrocytic development of the malaria parasite Plasmodium falciparum. Biochem Biophys Res Commun 446:125-31.

42. Flueck C, Drought LG, Jones A, Patel A, Perrin AJ, Walker EM, Nofal SD, Snijders AP, Blackman MJ, Baker DA. 2019. Phosphodiesterase beta is the master regulator of cAMP signalling during malaria parasite invasion. PLoS Biol 17:e3000154.

43. Patel A, Perrin AJ, Flynn HR, Bisson C, Withers-Martinez C, Treeck M, Flueck C, Nicastro G, Martin SR, Ramos A, Gilberger TW, Snijders AP, Blackman MJ, Baker DA. 2019. Cyclic AMP signalling controls key components of malaria parasite host cell invasion machinery. PLoS Biol 17:e3000264.
44. Jia Y, Marq JB, Bisio H, Jacot D, Mueller C, Yu L, Choudhary J, Brochet M, Soldati-Favre D. 2017. Crosstalk between PKA and PKG controls pH-dependent host cell egress of Toxoplasma gondii. EMBO J 36:3250-3267.
45. Uboldi AD, Wilde ML, McRae EA, Stewart RJ, Dagley LF, Yang L, Katris NJ, Hapuarachchi SV, Coffey MJ, Lehane AM, Botte CY, Waller RF, Webb AI, McConville MJ, Tonkin CJ. 2018. Protein kinase A negatively regulates Ca2+ signalling in Toxoplasma gondii. PLoS Biol 16:e2005642.
46. Soderling SH, Beavo JA. 2000. Regulation of cAMP and cGMP signaling: new phosphodiesterases and new functions. Curr Opin Cell Biol 12:174-9.
47. Yuasa K, Mi-Ichi F, Kobayashi T, Yamanouchi M, Kotera J, Kita K, Omori K. 2005. PfPDE1, a novel cGMP-specific phosphodiesterase from the human malaria parasite Plasmodium falciparum. Biochem J 392:221-9.
48. Howard BL, Harvey KL, Stewart RJ, Azevedo MF, Crabb BS, Jennings IG, Sanders PR, Manallack DT, Thompson PE, Tonkin CJ, Gilson PR. 2015. Identification of potent phosphodiesterase inhibitors that demonstrate cyclic nucleotide-dependent functions in apicomplexan parasites. ACS Chem Biol 10:1145-54.
49. Kebaier C, Vanderberg JP. 2010. Initiation of Plasmodium sporozoite motility by albumin is associated with induction of intracellular signalling. Int J Parasitol 40:25-33.
50. Sugi T, Ma YF, Tomita T, Murakoshi F, Eaton MS, Yakubu R, Han B, Tu V, Kato K, Kawazu S, Gupta N, Suvorova ES, White MW, Kim K, Weiss LM. 2016. Toxoplasma gondii Cyclic AMP-Dependent Protein Kinase Subunit 3 Is Involved in the Switch from Tachyzoite to Bradyzoite Development. MBio 7.
51. Baker DA, Drought LG, Flueck C, Nofal SD, Patel A, Penzo M, Walker EM. 2017. Cyclic nucleotide signalling in malaria parasites. Open Biol 7.
52. Hehl AB, Basso WU, Lippuner C, Ramakrishnan C, Okoniewski M, Walker RA, Grigg ME, Smith NC, Deplazes P. 2015. Asexual expansion of Toxoplasma gondii merozoites is distinct from tachyzoites and entails expression of non-overlapping gene families to attach, invade, and replicate within feline enterocytes. BMC Genomics 16:66.
53. Vo KC, Gunay-Esiyok O, Liem N, Gupta N. 2020. The protozoan parasite Toxoplasma gondii encodes a gamut of phosphodiesterases during its lytic cycle in human cells. Comput Struct Biotechnol J 18:3861-3876.
54. Sidik SM, Huet D, Ganesan SM, Huynh MH, Wang T, Nasamu AS, Thiru P, Saeij JPJ, Carruthers VB, Niles JC, Lourido S. 2016. A Genome-wide CRISPR Screen in Toxoplasma Identifies Essential Apicomplexan Genes. Cell 166:1423-1435 e12.
55. Lu S, Wang J, Chitsaz F, Derbyshire MK, Geer RC, Gonzales NR, Gwadz M, Hurwitz DI, Marchler GH, Song JS, Thanki N, Yamashita RA, Yang M, Zhang D, Zheng C, Lanczycki CJ, Marchler-Bauer A. 2020. CDD/SPARCLE: the conserved domain database in 2020. Nucleic Acids Res 48:D265-D268.

56. Schultz JE. 2009. Structural and biochemical aspects of tandem GAF domains. Handb Exp Pharmacol doi:10.1007/978-3-540-68964-5_6:93-109.
57. Tsirigos KD, Peters C, Shu N, Kall L, Elofsson A. 2015. The TOPCONS web server for consensus prediction of membrane protein topology and signal peptides. Nucleic Acids Res 43:W401-7.
58. Shen B, Brown KM, Lee TD, Sibley LD. 2014. Efficient gene disruption in diverse strains of Toxoplasma gondii using CRISPR/CAS9. MBio 5:e01114-14.
59. Brown KM, Long S, Sibley LD. 2018. Conditional Knockdown of Proteins Using Auxin-inducible Degron (AID) Fusions in Toxoplasma gondii. Bio Protoc 8.
60. Kambara H, Liu F, Zhang X, Liu P, Bajrami B, Teng Y, Zhao L, Zhou S, Yu H, Zhou W, Silberstein LE, Cheng T, Han M, Xu Y, Luo HR. 2018. Gasdermin D Exerts Anti-inflammatory Effects by Promoting Neutrophil Death. Cell Rep 22:2924-2936.
61. Rath A, Glibowicka M, Nadeau VG, Chen G, Deber CM. 2009. Detergent binding explains anomalous SDS-PAGE migration of membrane proteins. Proceedings of the National Academy of Sciences 106:1760-1765.
62. Matsumoto H, Haniu H, Komori N. 2019. Determination of Protein Molecular Weights on SDS-PAGE. Methods Mol Biol 1855:101-105.
63. Mueller C, Samoo A, Hammoudi PM, Klages N, Kallio JP, Kursula I, Soldati-Favre D. 2016. Structural and functional dissection of Toxoplasma gondii armadillo repeats only protein. J Cell Sci 129:1031-45.
64. Laemmli UK. 1970. Cleavage of structural proteins during the assembly of the head of bacteriophage T4. Nature 227:680-5.

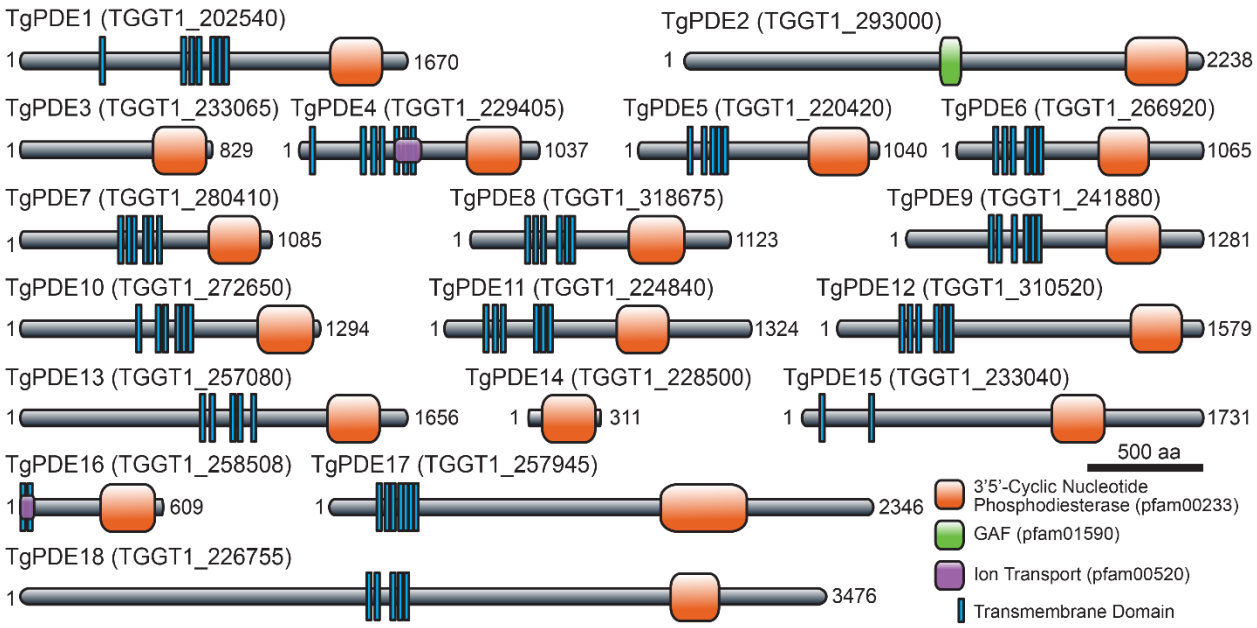

Fig 1 Predicted protein domain architecture of the TgPDE family. Transmembrane domains and conserved protein domains of the 18 putative 3'5'-cyclic nucleotide phosphodiesterases in *T. gondii* based on TOPCONS and NCBI Conserved Domain Database searches.

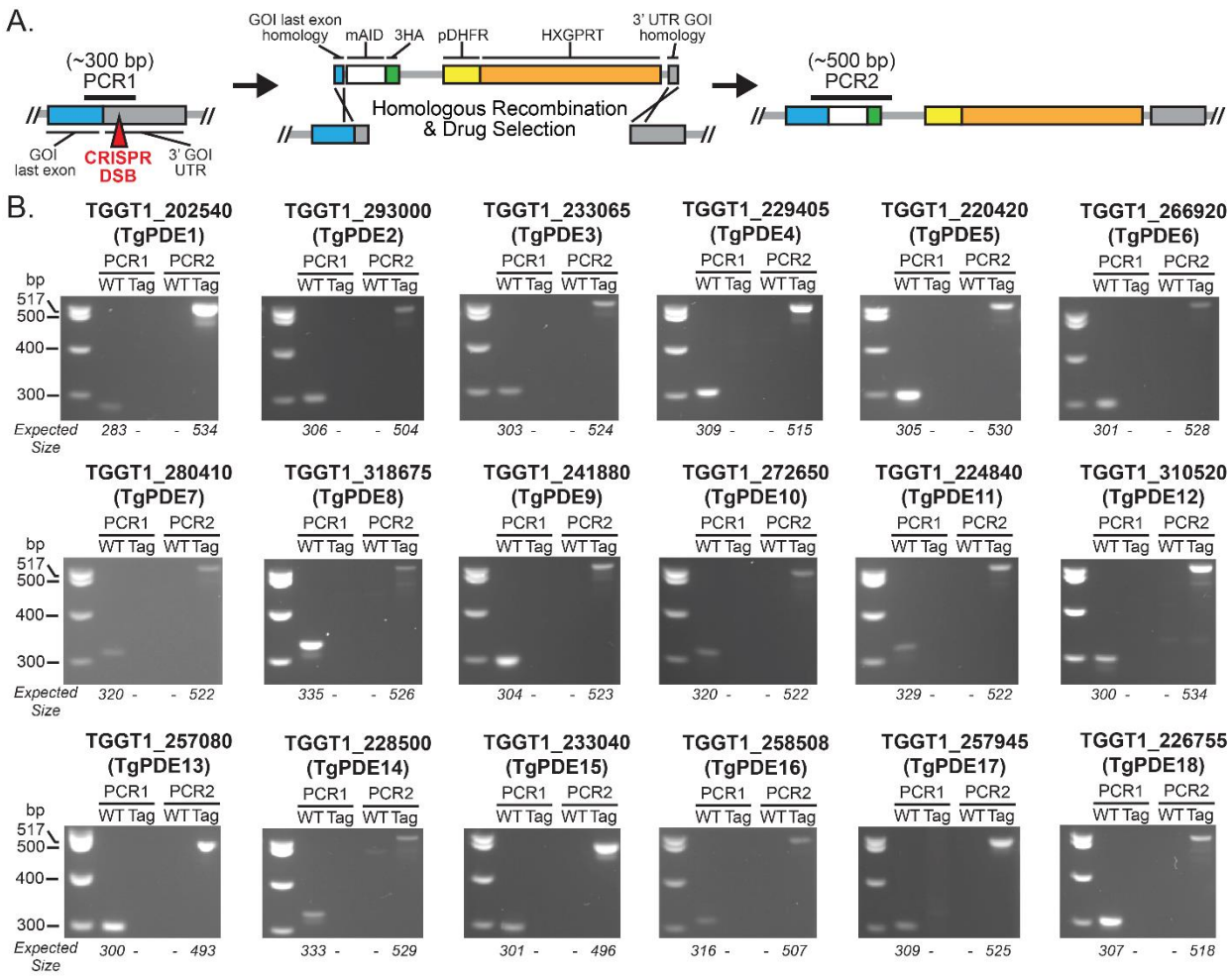

Fig 2 Creation of conditional knockdown lines for all 18 TgPDEs. (A) CRISPR/Cas9 genome editing strategy used to append an *mAID-3HA, HXGPRT* cassette (with 40 bp homology flanks) to the 3' end of each *TgPDE* gene in the RH TIR1-3FLAG background. (B) Diagnostic PCR confirmation of successful *mAID-3HA, HXGPRT* integration for each *TgPDE* gene. Differential genomic positions of PCR1 and PCR2 are shown in (A). WT, wild type parental line RH TIR1-3FLAG. Tag, specific RH TgPDE-mAID-3HA clone.

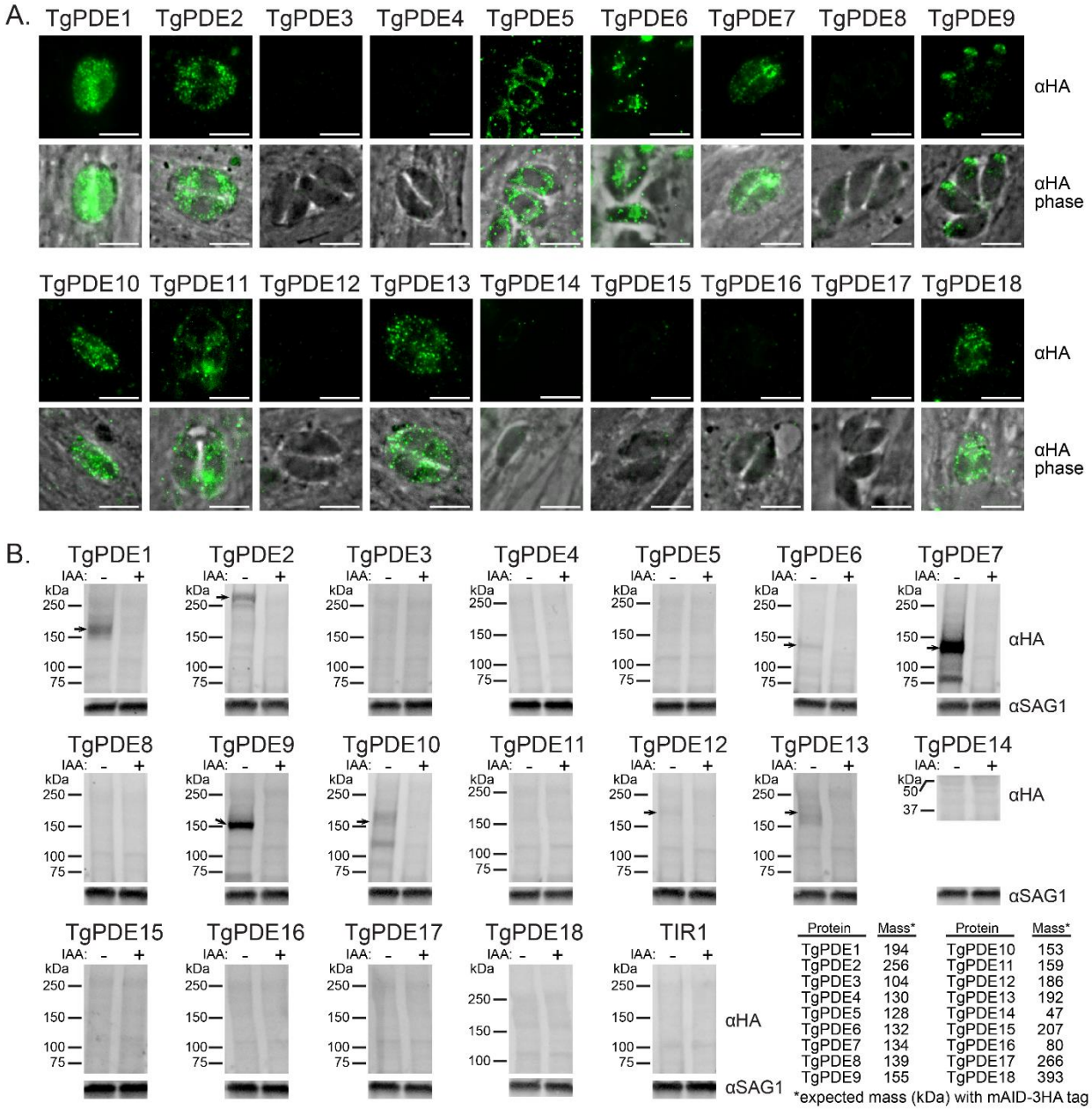

Fig 3 Expression and depletion of TgPDE-mAID-3HA fusions in tachyzoites. (A) IF microscopy of intracellular RH TgPDE-mAID-3HA parasites labeled with mouse anti-HA (1:1000) and goat anti-mouse IgG Alexa Fluor 488 (1:2000). Scale bar = 5 μm. (B) Immunoblots of lysates from RH TIR1-3FLAG (TIR1) and RH TgPDE-mAID-3HA (TgPDE) parasites treated with vehicle (EtOH) or 0.5 mM auxin (IAA) for 18 h. Blots probed with mouse anti-HA (1:1000), rabbit anti-SAG1 (1:10000), goat anti-mouse-

AFP800 (1:2000), and goat anti-rabbit-AFP680 (1:2000). Table indicates predicted total mass of each TgPDE including their mAID-3HA tag (12 kDa). Arrows indicate IB-detectable TgPDE-mAID-3HA fusions in tachyzoites.

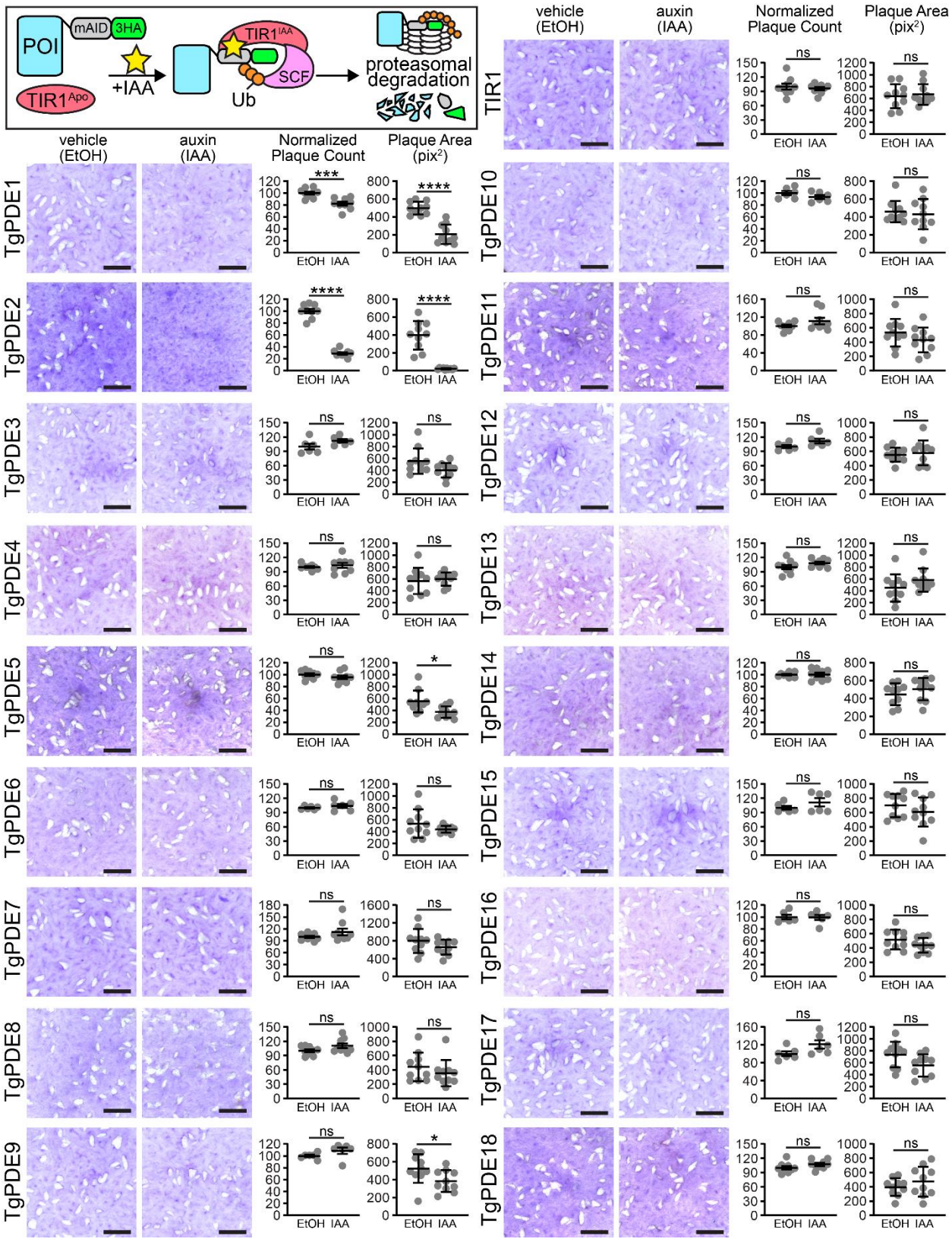
POI
mAID
3HA
TIR1Apo
+IAA
TIR1IAA
SCF
Ub
proteasomal degradation
vehicle (EtOH)
auxin (IAA)
Normalized Plaque Count
Plaque Area (pix²)
TIR1
TgPDE1
TgPDE2
TgPDE3
TgPDE4
TgPDE5
TgPDE6
TgPDE7
TgPDE8
TgPDE9
TgPDE10
TgPDE11
TgPDE12
TgPDE13
TgPDE14
TgPDE15
TgPDE16
TgPDE17
TgPDE18
EtOH
IAA
ns
*
***
****

834

Fig 4 Contribution of each TgPDE to tachyzoite growth. Inset: Auxin-inducible protein degradation. Plaques formed on HFF monolayers by RH TIR1-3FLAG (TIR1) or derivative RH TgPDE-mAID-3HA lines treated with vehicle (EtOH) or 0.5 mM auxin (IAA) for 8 days. Scale bar = 5 mm. Plaque count data represented as mean ± SD (n = 6 or 9 replicates combined from N = 2 or 3 trials, respectively. For baseline consistency, plaque counts were normalized to 100 vehicle treated plaques for each line. Plaque area data represented as mean ± SD (n = 10) from the representative images shown. Unpaired student's t test (ethanol vs IAA), *P*: * ≤ 0.05, *** ≤ 0.001, **** ≤ 0.0001.

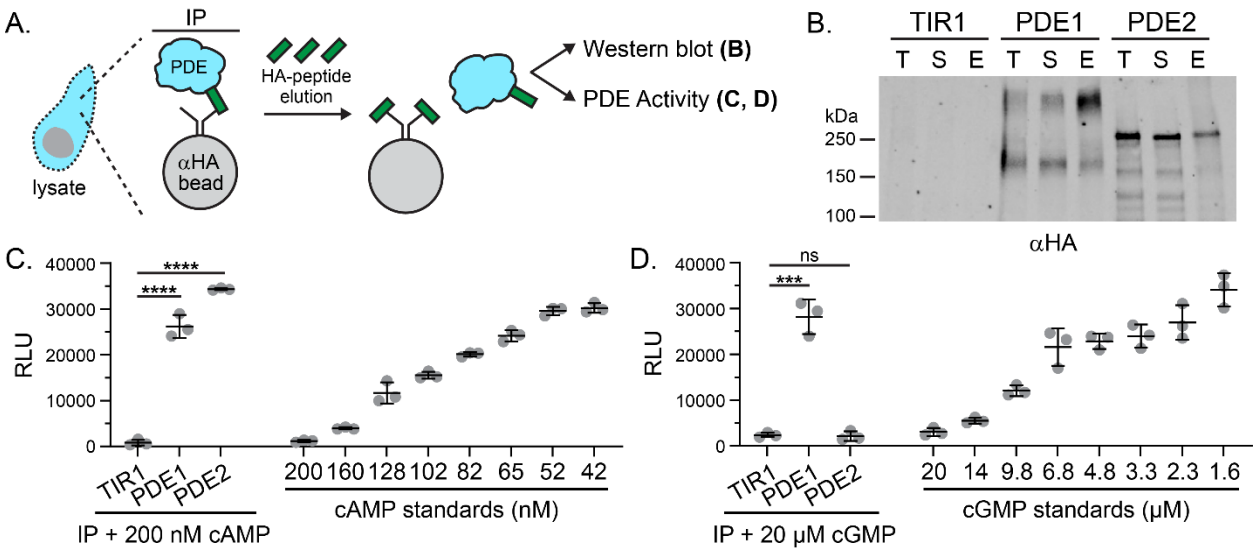

Fig 5 Phosphodiesterase activity of immunoprecipitated TgPDE1 and TgPDE2. (A) Immunoprecipitation strategy for purifying tagged TgPDE1 and TgPDE2 proteins from tachyzoite native lysates. Untagged parental line RH TIR1-3FLAG (TIR1) served as negative control. (B) Representative immunoblot of immunoprecipitation fractions probed with rat anti-HA (1:1000) and goat anti-rat IRDye 800CW (1:5000). T = total lysate, S = soluble lysate, E = eluate. (C) Cyclic AMP phosphodiesterase activity of immunoprecipitated elution fractions incubated 1:1 with 0.2 μM cAMP for 2 h at 37°C. Standards shown were incubated 1:1 with PDE storage buffer for 2 h at 37°C. (D) Cyclic GMP phosphodiesterase activity of immunoprecipitated elution fractions incubated 1:1 with 20 μM cGMP for 2 h at 37°C. Standards shown were incubated 1:1 with PDE storage buffer for 2 h at 37°C. (C,D) Data represented as mean ± SD (n = 3) from one of four trials (N=4) with similar outcomes. Statistical significance was determined using an unpaired student's t test (TIR1 vs TgPDE1; TIR1 vs TgPDE2), *P*: *** ≤ 0.001, **** ≤ 0.0001.

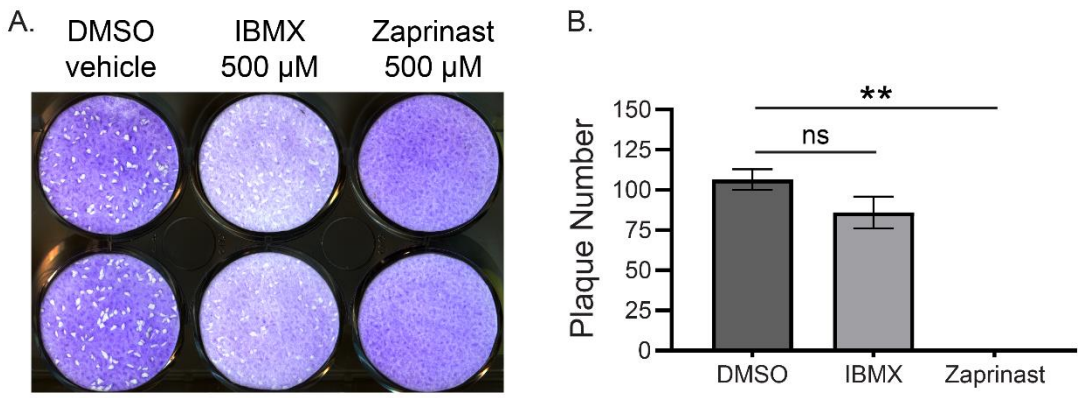

FIG S1 Pharmacological evidence for the importance of TgPDEs. (A) Plaques formed on HFF monolayers by 200 RH TIR1-3FLAG tachyzoites treated with vehicle (DMSO) or 0.5 mM PDE inhibitors (IBMX or zaprinast) for 8 days. (B) Quantification of plaques shown in A, mean ± SD (n = 2). Statistical significance was determined using an unpaired student's t test comparing plaque formation in the presence of PDE inhibitors vs vehicle, $^{**}P \leq 0.01$.

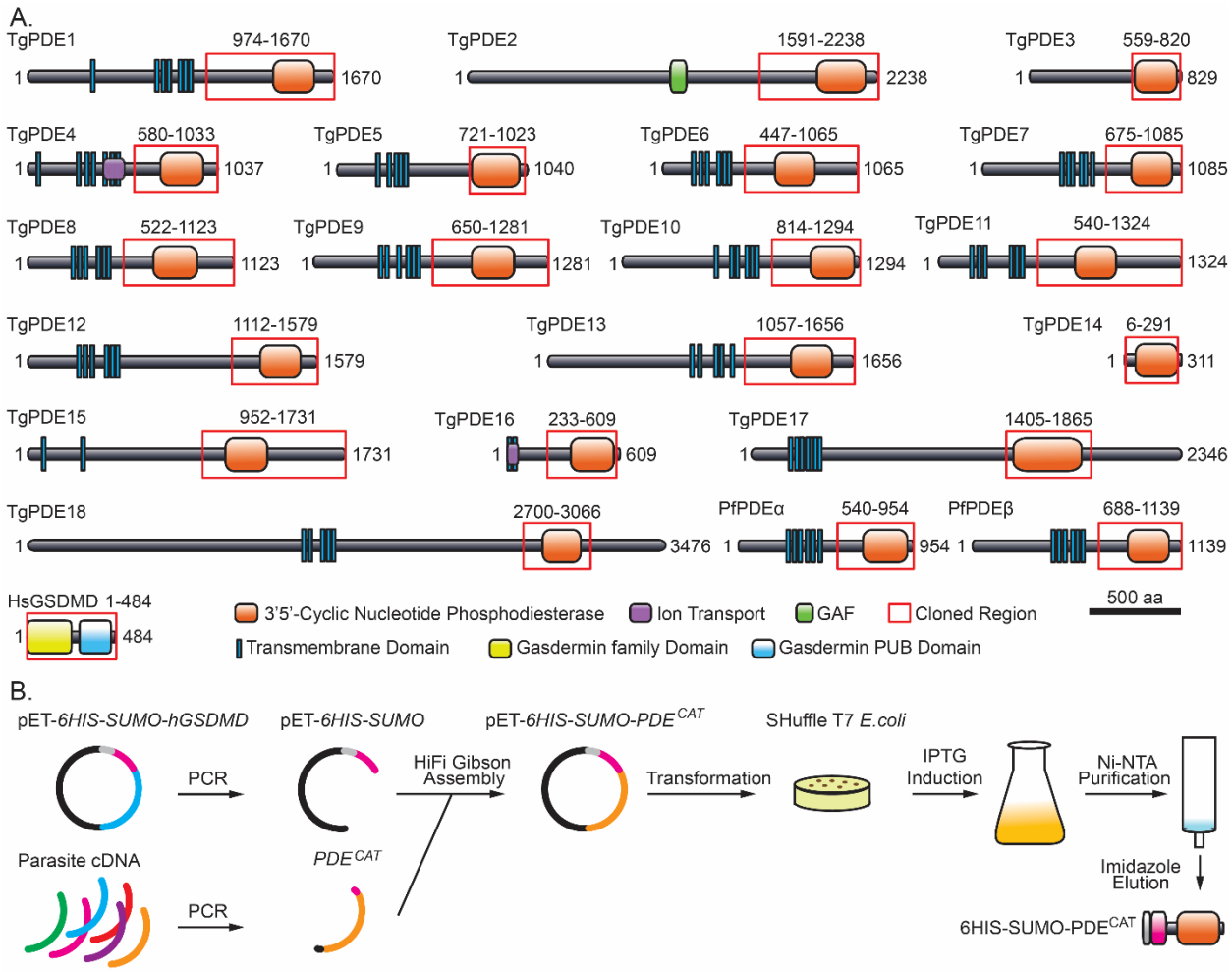

FIG S2 Strategy for production of recombinant TgPDE catalytic fragments. Related to FIG S3-4. (A) Cloned regions (outlined in red) for 18 TgPDEs, 2 PfPDEs (+ controls), and human gasdermin D (hGSDMD) protein (- control). (B) Cloning, transformation, induction, and purification of recombinant 6HIS-SUMO protein fusions in *E. coli*.

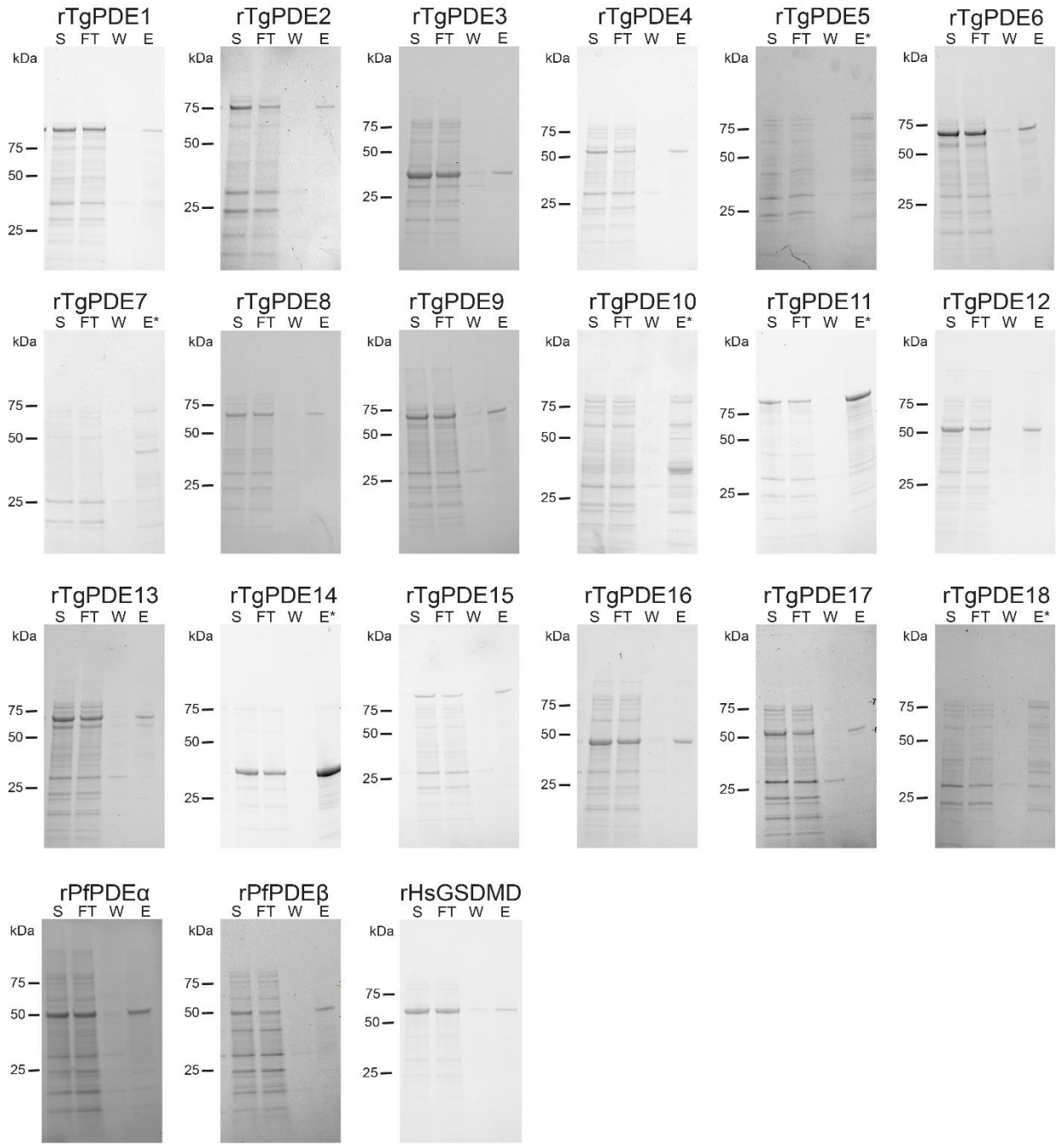

FIG S3 SDS-PAGE analysis of recombinant TgPDE catalytic fragments. Related to FIG S2, FIG S4. Homogenized inclusion body fractions from IPTG-induced *E. coli* expressing 6HIS-SUMO protein fusions were solubilized with sarkosyl and partially purified using immobilized metal affinity chromatography (Ni-NTA). Recombinant protein fractions from a representative experiment were resolved on a 4-20% SDS-PAGE gel

containing total protein fluorescent dye for imaging. S, soluble lysate; FT, flowthrough; W, combined washes; E, 1:10 diluted imidazole eluate (recombinant protein); E*, undiluted imidazole eluate.

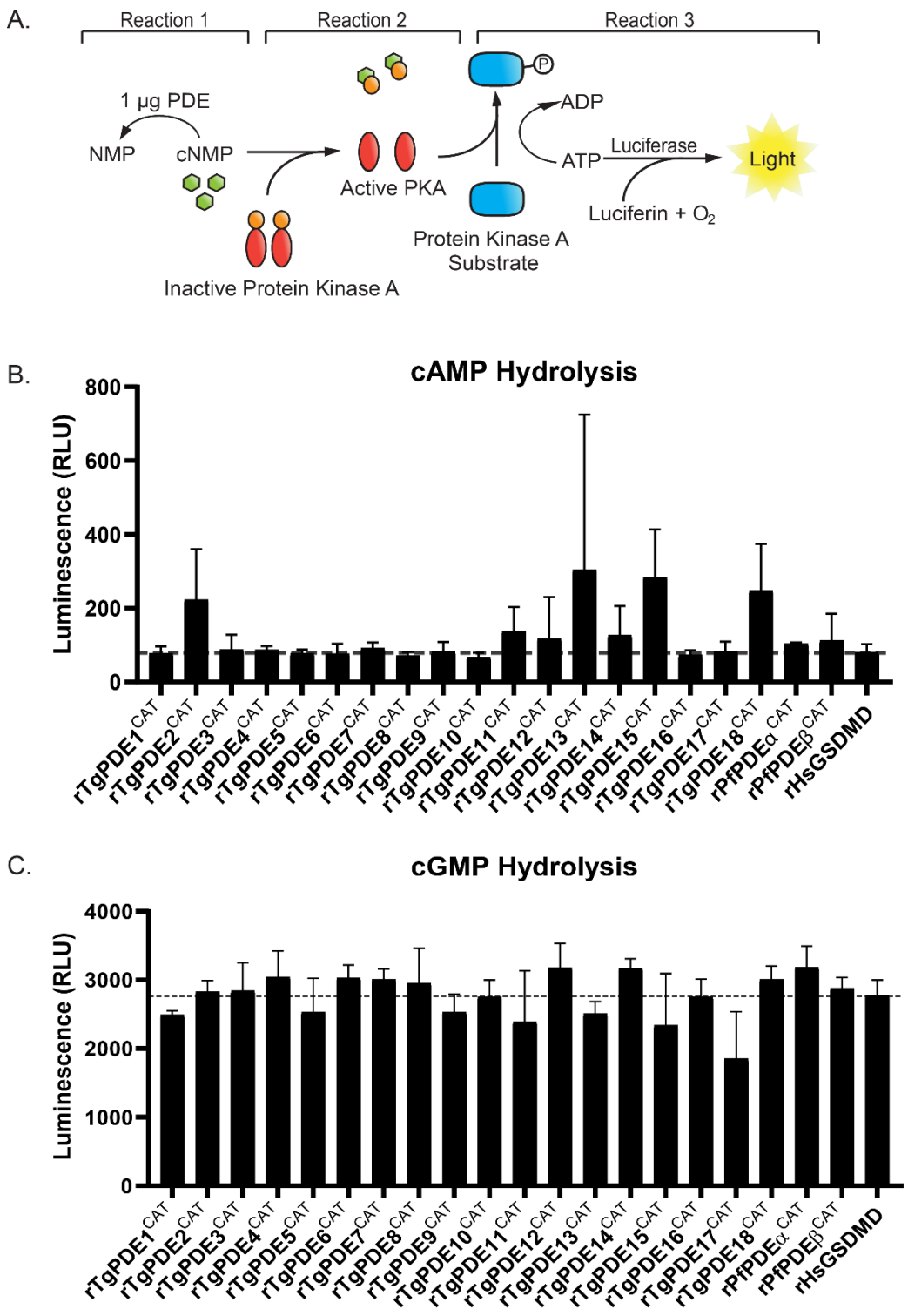

FIG S4 Phosphodiesterase activities of recombinant TgPDE catalytic fragments. Related to FIG S2-3. (A) Strategy to determine phosphodiesterase activity of recombinant PDEs (6HIS-SUMO fusions) using the PDE-Glo system where relative

luminescence (RLU) is proportional to cyclic nucleotide hydrolysis. (B) Cyclic AMP phosphodiesterase activity of 1 µg recombinant proteins incubated 1:1 with 2 µM cAMP for 2 h at 37°C. (C) Cyclic GMP phosphodiesterase activity of 1 µg recombinant proteins incubated 1:1 with 20 µM cGMP for 2 h at 37°C. (B,C) Dotted lines represent the baseline activity threshold of the negative control, recombinant human gasdermin D (rHsGSDMD). A single trial of several similar trials is shown. Error bars indicate the standard deviation of 3 technical replicates.

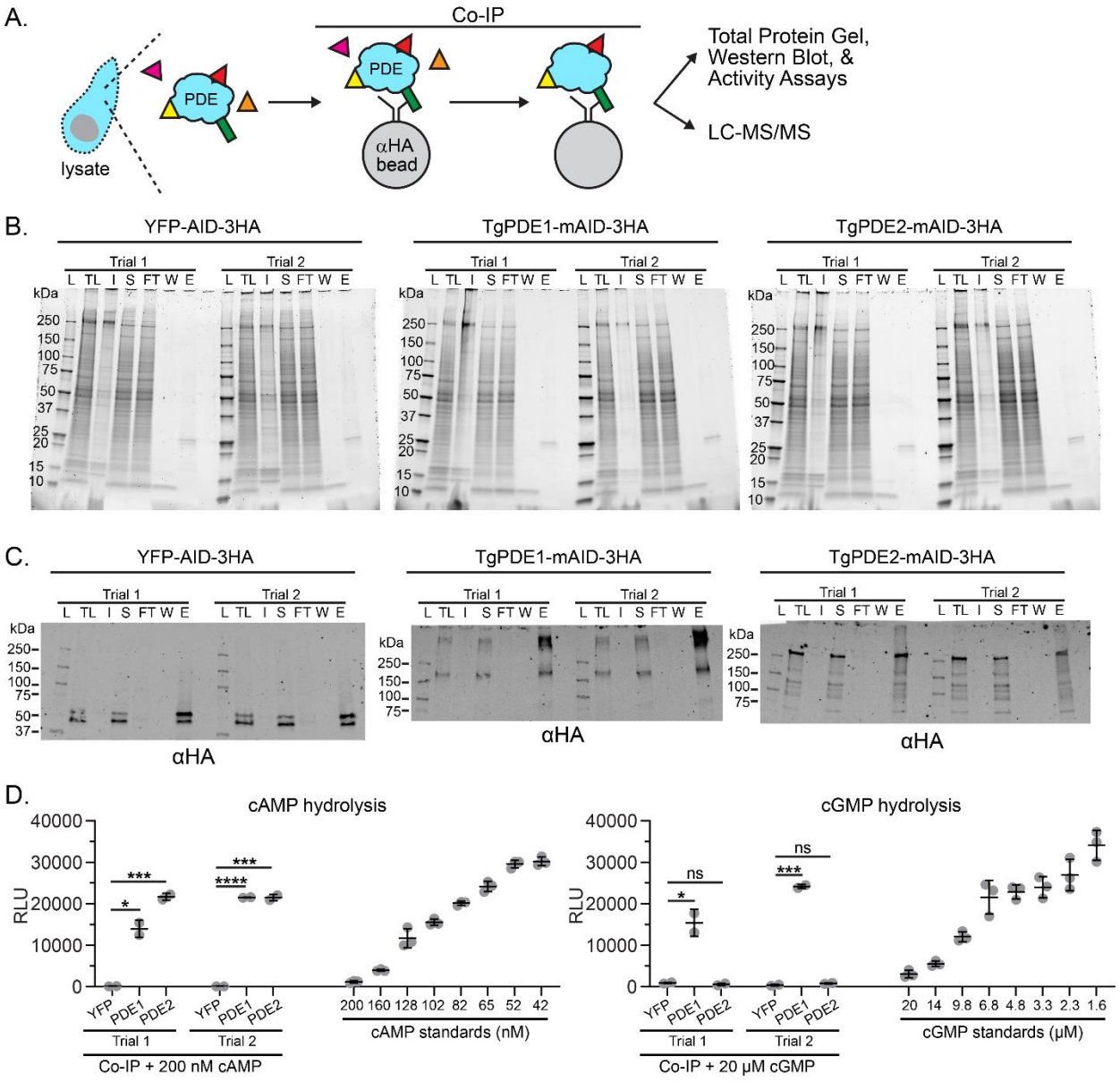
A.
Co-IP
PDE
PDE
αHA bead
lysate
Total Protein Gel, Western Blot, & Activity Assays
LC-MS/MS
B.
YFP-AID-3HA
TgPDE1-mAID-3HA
TgPDE2-mAID-3HA
Trial 1
Trial 2
L TL I S FT W E
kDa
250
150
100
75
50
37
25
20
15
10
C.
YFP-AID-3HA
TgPDE1-mAID-3HA
TgPDE2-mAID-3HA
αHA
D.
cAMP hydrolysis
cGMP hydrolysis
RLU
40000
30000
20000
10000
0
YFP
PDE1
PDE2
Trial 1
Trial 2
Co-IP + 200 nM cAMP
Co-IP + 20 μM cGMP
200 160 128 102 82 65 52 42
cAMP standards (nM)
20 14 9.8 6.8 4.8 3.3 2.3 1.6
cGMP standards (μM)
ns

896

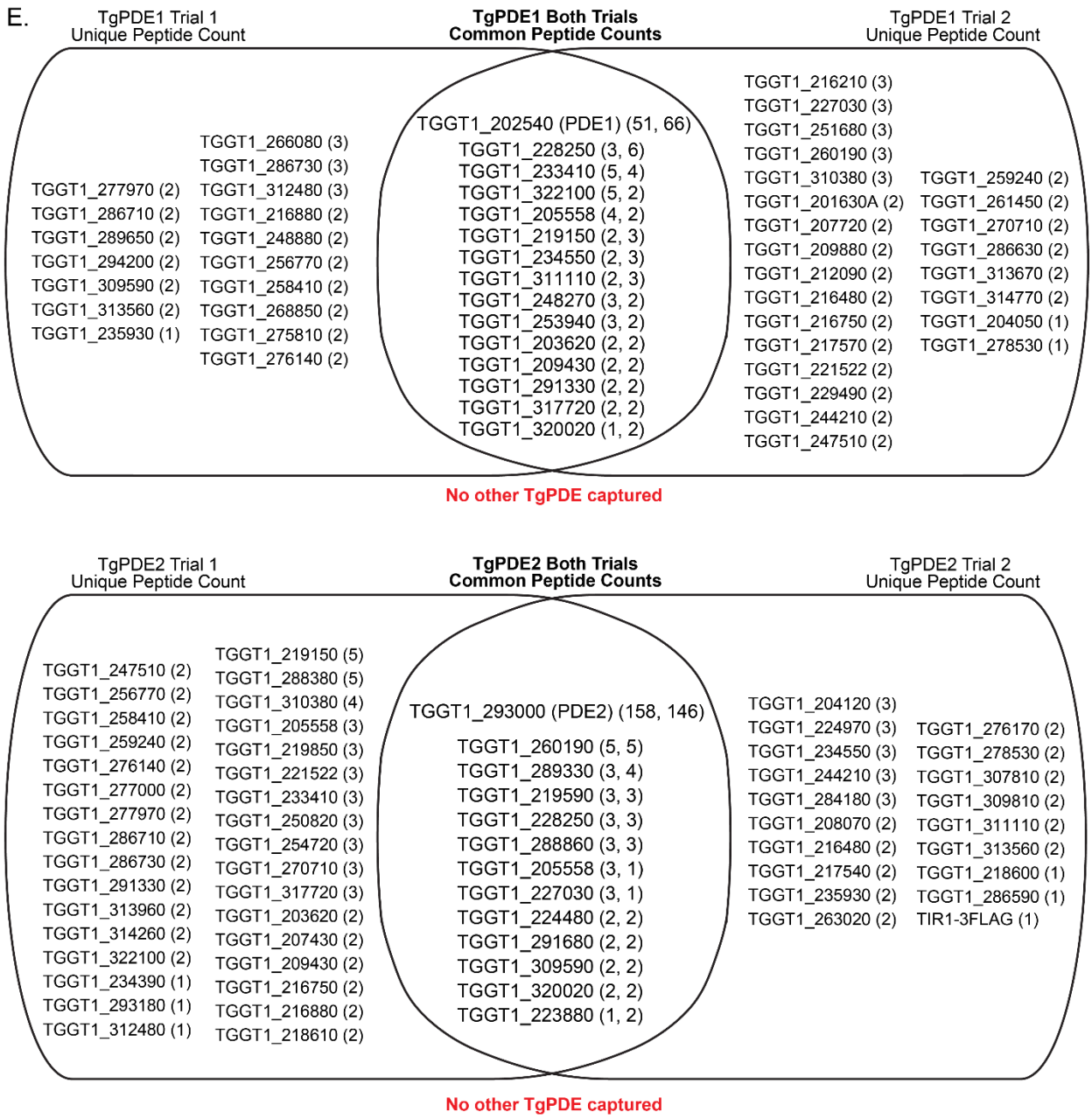

FIG S5 Protein interactomes of TgPDE1 and TgPDE2. (A) Schematic of co-immunoprecipitation of mAID-3HA fusions with anti-HA magnetic beads and downstream applications. (B) SDS-PAGE analysis of total protein in co-immunoprecipitation fractions using Oriole staining. L = ladder, TL = total lysate, I = insoluble lysate, S = soluble lysate, FT = flowthrough, W = combined washes, E = eluate. (C) Immunoblot analysis of co-immunoprecipitation fractions probed with rat anti-

HA (1:1000) and goat anti-rat IRDye 800CW (1:5000). (D) Left, cAMP phosphodiesterase activity of immunoprecipitated elution fractions incubated 1:1 with 0.2 µM cAMP for 2h at 37°C. Standards shown were incubated 1:1 with PDE storage buffer for 2 h at 37°C. Right, cGMP phosphodiesterase activity of immunoprecipitated elution fractions incubated 1:1 with 20 µM cGMP for 2h at 37°C. Standards shown were incubated 1:1 with PDE storage buffer for 2 h at 37°C. Data represented as mean ± SD (n = 3) for each trial shown. Statistical significance was determined using an unpaired student's t test comparing phosphodiesterase activity between PDE fractions and YFP (negative control). *P*: * ≤ 0.05, *** ≤ 0.001, **** ≤ 0.0001. (E) LC-MS/MS identification of protein interactors of TgPDE1 and TgPDE2 from two independent co-immunoprecipitation trials. Shown are the gene accessions with unique peptide counts for each protein identified (not found in YFP negative control). No other TgPDEs co-purified with TgPDE1 or TgPDE2.

Table S1 *Toxoplasma* strains used in this study.

Strain Name	Genotype	Source
RH	RH	ATCC #50838
GT1	GT1	L. David Sibley Laboratory (WUSTL)
RH TIR1-3FLAG	RH*Δhxgprt*Δ*ku80; TUB1:TIR1-3FLAG, SAG1:CAT*	Brown et al., 2017; Long et al., 2017
RH PDE1-mAID-3HA	RH*Δhxgprt*Δ*ku80; TUB1:TIR1-3FLAG, SAG1:CAT; PDE1-mAID-3HA, DHFR-TS:HXGPRT*	This work
RH PDE2-mAID-3HA	RH*Δhxgprt*Δ*ku80; TUB1:TIR1-3FLAG, SAG1:CAT; PDE2-mAID-3HA, DHFR-TS:HXGPRT*	This work
RH PDE3-mAID-3HA	RH*Δhxgprt*Δ*ku80; TUB1:TIR1-3FLAG, SAG1:CAT; PDE3-mAID-3HA, DHFR-TS:HXGPRT*	This work
RH PDE4-mAID-3HA	RH*Δhxgprt*Δ*ku80; TUB1:TIR1-3FLAG, SAG1:CAT; PDE4-mAID-3HA, DHFR-TS:HXGPRT*	This work
RH PDE5-mAID-3HA	RH*Δhxgprt*Δ*ku80; TUB1:TIR1-3FLAG, SAG1:CAT; PDE5-mAID-3HA, DHFR-TS:HXGPRT*	This work
RH PDE6-mAID-3HA	RH*Δhxgprt*Δ*ku80; TUB1:TIR1-3FLAG, SAG1:CAT; PDE6-mAID-3HA, DHFR-TS:HXGPRT*	This work
RH PDE7-mAID-3HA	RH*Δhxgprt*Δ*ku80; TUB1:TIR1-3FLAG, SAG1:CAT; PDE7-mAID-3HA, DHFR-TS:HXGPRT*	This work
RH PDE8-mAID-3HA	RH*Δhxgprt*Δ*ku80; TUB1:TIR1-3FLAG, SAG1:CAT; PDE8-mAID-3HA, DHFR-TS:HXGPRT*	This work
RH PDE9-mAID-3HA	RH*Δhxgprt*Δ*ku80; TUB1:TIR1-3FLAG, SAG1:CAT; PDE9-mAID-3HA, DHFR-TS:HXGPRT*	This work
RH PDE10-mAID-3HA	RH*Δhxgprt*Δ*ku80; TUB1:TIR1-3FLAG, SAG1:CAT; PDE10-mAID-3HA, DHFR-TS:HXGPRT*	This work
RH PDE11-mAID-3HA	RH*Δhxgprt*Δ*ku80; TUB1:TIR1-3FLAG, SAG1:CAT; PDE11-mAID-3HA, DHFR-TS:HXGPRT*	This work
RH PDE12-mAID-3HA	RH*Δhxgprt*Δ*ku80; TUB1:TIR1-3FLAG, SAG1:CAT; PDE12-mAID-3HA, DHFR-TS:HXGPRT*	This work
RH PDE13-mAID-3HA	RH*Δhxgprt*Δ*ku80; TUB1:TIR1-3FLAG, SAG1:CAT; PDE13-mAID-3HA, DHFR-TS:HXGPRT*	This work
RH PDE14-mAID-3HA	RH*Δhxgprt*Δ*ku80; TUB1:TIR1-3FLAG, SAG1:CAT; PDE14-mAID-3HA, DHFR-TS:HXGPRT*	This work
RH PDE15-mAID-3HA	RH*Δhxgprt*Δ*ku80; TUB1:TIR1-3FLAG, SAG1:CAT; PDE15-mAID-3HA, DHFR-TS:HXGPRT*	This work
RH PDE16-mAID-3HA	RH*Δhxgprt*Δ*ku80; TUB1:TIR1-3FLAG, SAG1:CAT; PDE16-mAID-3HA, DHFR-TS:HXGPRT*	This work
RH PDE17-mAID-3HA	RH*Δhxgprt*Δ*ku80; TUB1:TIR1-3FLAG, SAG1:CAT; PDE17-mAID-3HA, DHFR-TS:HXGPRT*	This work
RH PDE18-mAID-3HA	RH*Δhxgprt*Δ*ku80; TUB1:TIR1-3FLAG, SAG1:CAT; PDE18-mAID-3HA, DHFR-TS:HXGPRT*	This work
RH YFP-AID-3HA	RH*Δhxgprt*Δ*ku80; TUB1:TIR1-3FLAG, SAG1:CAT; TUB1:YFP-AID-3HA, DHFR-TS:HXGPRT*	(Long et al., 2017)

921 **Table S2** Plasmids used in this study.

p#	Plasmid Name	Description	Usage	Source
p1	p*TUB1:YFP-mAID-3HA, DHFR-TS:HXGPRT*	*YFP-mAID-3HA* fusion driven by a minimal *TgTUB1* promoter with an *TgHXGPRT* drug selectable marker.	PCR template for generating *TgPDE-mAID-3HA* tagging amplicons.	Brown et al. 2017
p2	p*SAG1:Cas9-GFP, U6:_gRNA*	Linear *SpCas9-GFP*, *gRNA* (no protospacer) destination vector	Linear *Cas9-GFP, gRNA* (no protospacer) destination vector for inserting *GOI protospacer* by ssDNA (59-60mer) HiFi assembly	Shen et al. 2014
p3	p*SAG1:Cas9-GFP, U6:sg202540(PDE1) 3'UTR*	*Streptococcus pyogenes Cas9* fused to *GFP* driven by a *TgSAG1* promoter and *CRISPR sgRNA targeting TgPDE1 3' UTR* driven from a *Pol III TgU6* promoter	Co-transfection with *TgPDE1-mAID-3HA, DHFR:HXGPRT* amplicon for CRISPR/Cas9 tagging C-terminus of TgPDE1.	This work
p4	p*SAG1:Cas9-GFP, U6:sg293000(PDE2) 3'UTR*	*Streptococcus pyogenes Cas9* fused to *GFP* driven by a *TgSAG1* promoter and *CRISPR sgRNA targeting TgPDE2 3' UTR* driven from a *Pol III TgU6* promoter	Co-transfection with *TgPDE2-mAID-3HA, DHFR:HXGPRT* amplicon for CRISPR/Cas9 tagging C-terminus of TgPDE2.	This work
p5	p*SAG1:Cas9-GFP, U6:sg233065(PDE3) 3'UTR*	*Streptococcus pyogenes Cas9* fused to *GFP* driven by a *TgSAG1* promoter and *CRISPR sgRNA targeting TgPDE3 3' UTR* driven from a *Pol III TgU6* promoter	Co-transfection with *TgPDE3-mAID-3HA, DHFR:HXGPRT* amplicon for CRISPR/Cas9 tagging C-terminus of TgPDE3.	This work
p6	p*SAG1:Cas9-GFP, U6:sg229405(PDE4) 3'UTR*	*Streptococcus pyogenes Cas9* fused to *GFP* driven by a *TgSAG1* promoter and *CRISPR sgRNA targeting TgPDE4 3' UTR* driven from a *Pol III TgU6* promoter	Co-transfection with *TgPDE4-mAID-3HA, DHFR:HXGPRT* amplicon for CRISPR/Cas9 tagging C-terminus of TgPDE4.	This work
p7	p*SAG1:Cas9-GFP, U6:sg220420(PDE5) 3'UTR*	*Streptococcus pyogenes Cas9* fused to *GFP* driven by a *TgSAG1* promoter and *CRISPR sgRNA targeting TgPDE5 3' UTR* driven from a *Pol III TgU6* promoter	Co-transfection with *TgPDE5-mAID-3HA, DHFR:HXGPRT* amplicon for CRISPR/Cas9 tagging C-terminus of *Tg*PDE5.	This work
p8	p*SAG1:Cas9-GFP, U6:sg266920(PDE6) 3'UTR*	*Streptococcus pyogenes Cas9* fused to *GFP* driven by a *TgSAG1* promoter and *CRISPR sgRNA targeting TgPDE6 3' UTR* driven from a *Pol III TgU6* promoter	Co-transfection with *TgPDE6-mAID-3HA, DHFR:HXGPRT* amplicon for CRISPR/Cas9 tagging C-terminus of TgPDE6.	This work
p9	p*SAG1:Cas9-GFP, U6:sg280410(PDE7) 3'UTR*	*Streptococcus pyogenes Cas9* fused to *GFP* driven by a *TgSAG1* promoter and *CRISPR sgRNA targeting TgPDE7 3' UTR* driven from a *Pol III TgU6* promoter	Co-transfection with *TgPDE7-mAID-3HA, DHFR:HXGPRT* amplicon for CRISPR/Cas9 tagging C-terminus of TgPDE7.	This work
p10	p*SAG1:Cas9-GFP, U6:sg318675(PDE8) 3'UTR*	*Streptococcus pyogenes Cas9* fused to *GFP* driven by a *TgSAG1* promoter and *CRISPR sgRNA targeting TgPDE8 3' UTR* driven from a *Pol III TgU6* promoter	Co-transfection with *TgPDE8-mAID-3HA, DHFR:HXGPRT* amplicon for CRISPR/Cas9 tagging C-terminus of TgPDE8.	This work
p11	p*SAG1:Cas9-GFP, U6:sg241880(PDE9) 3'UTR*	*Streptococcus pyogenes Cas9* fused to *GFP* driven by a *TgSAG1* promoter and *CRISPR sgRNA targeting TgPDE9 3' UTR* driven from a *Pol III TgU6* promoter	Co-transfection with *TgPDE9-mAID-3HA, DHFR:HXGPRT* amplicon for CRISPR/Cas9 tagging C-terminus of TgPDE9.	This work
p12	p*SAG1:Cas9-GFP, U6:sg272650(PDE10) 3'UTR*	*Streptococcus pyogenes Cas9* fused to *GFP* driven by a *TgSAG1* promoter and *CRISPR sgRNA targeting TgPDE10 3' UTR* driven from a *Pol III TgU6* promoter	Co-transfection with *TgPDE10-mAID-3HA, DHFR:HXGPRT* amplicon for CRISPR/Cas9 tagging C-terminus of TgPDE10.	This work
p13	p*SAG1:Cas9-GFP, U6:sg224840(PDE11) 3'UTR*	*Streptococcus pyogenes Cas9* fused to *GFP* driven by a *TgSAG1* promoter and *CRISPR sgRNA targeting TgPDE11 3' UTR* driven from a *Pol III TgU6* promoter	Co-transfection with *TgPDE11-mAID-3HA, DHFR:HXGPRT* amplicon for CRISPR/Cas9 tagging C-terminus of TgPDE11.	This work
p14	p*SAG1:Cas9-GFP, U6:sg310520(PDE12) 3'UTR*	*Streptococcus pyogenes Cas9* fused to *GFP* driven by a *TgSAG1* promoter and *CRISPR sgRNA targeting TgPDE12 3' UTR* driven from a *Pol III TgU6* promoter	Co-transfection with *TgPDE12-mAID-3HA, DHFR:HXGPRT* amplicon for CRISPR/Cas9 tagging C-terminus of TgPDE12.	This work

p#	Plasmid Name	Description	Usage	Source
p15	p*SAG1:Cas9-GFP, U6:sg257080(PDE13) 3'UTR*	*Streptococcus pyogenes Cas9* fused to *GFP* driven by a *TgSAG1* promoter and *CRISPR sgRNA targeting TgPDE13 3' UTR* driven from a *Pol III TgU6* promoter	Co-transfection with *TgPDE13-mAID-3HA, DHFR:HXGPRT* amplicon for CRISPR/Cas9 tagging C-terminus of TgPDE13.	This work
p16	p*SAG1:Cas9-GFP, U6:sg228500(PDE14) 3'UTR*	*Streptococcus pyogenes Cas9* fused to *GFP* driven by a *TgSAG1* promoter and *CRISPR sgRNA targeting TgPDE14 3' UTR* driven from a *Pol III TgU6* promoter	Co-transfection with *TgPDE14-mAID-3HA, DHFR:HXGPRT* amplicon for CRISPR/Cas9 tagging C-terminus of TgPDE14.	This work
p17	p*SAG1:Cas9-GFP, U6:sg233040(PDE15) 3'UTR*	*Streptococcus pyogenes Cas9* fused to *GFP* driven by a *TgSAG1* promoter and *CRISPR sgRNA targeting TgPDE15 3' UTR* driven from a *Pol III TgU6* promoter	Co-transfection with *TgPDE15-mAID-3HA, DHFR:HXGPRT* amplicon for CRISPR/Cas9 tagging C-terminus of TgPDE15.	This work
p18	p*SAG1:Cas9-GFP, U6:sg258508(PDE16) 3'UTR*	*Streptococcus pyogenes Cas9* fused to *GFP* driven by a *TgSAG1* promoter and *CRISPR sgRNA targeting TgPDE16 3' UTR* driven from a *Pol III TgU6* promoter	Co-transfection with *TgPDE16-mAID-3HA, DHFR:HXGPRT* amplicon for CRISPR/Cas9 tagging C-terminus of TgPDE16.	This work
p19	p*SAG1:Cas9-GFP, U6:sg257945(PDE17) 3'UTR*	*Streptococcus pyogenes Cas9* fused to *GFP* driven by a *TgSAG1* promoter and *CRISPR sgRNA targeting TgPDE17 3' UTR* driven from a *Pol III TgU6* promoter	Co-transfection with *TgPDE17-mAID-3HA, DHFR:HXGPRT* amplicon for CRISPR/Cas9 tagging C-terminus of TgPDE17.	This work
p20	p*SAG1:Cas9-GFP, U6:sg226755(PDE18) 3'UTR*	*Streptococcus pyogenes Cas9* fused to *GFP* driven by a *TgSAG1* promoter and *CRISPR sgRNA targeting TgPDE18 3' UTR* driven from a *Pol III TgU6* promoter	Co-transfection with *TgPDE18-mAID-3HA, DHFR:HXGPRT* amplicon for CRISPR/Cas9 tagging C-terminus of TgPDE18.	This work
p21	pET-*6HIS-SUMO-hGSDMD*	*E. coli* expression vector with a *KanR* drug selectable marker. Addgene #111559	Subcloning. Negative control protein for PDE assays	Addgene; Kambara et al. 2018
p22	pET-*6HIS-SUMO-TgPDE1*$^{974\text{-}1670}$	pET-*6HIS-SUMO-TgPDE1*$^{974\text{-}1670}$ driven by a *T7* promoter with a *KanR* drug selectable marker.	Expression and purification of recombinant TgPDE1$^{974\text{-}1670}$ from *E. coli*.	This work
p23	pET-*6HIS-SUMO-TgPDE2*$^{1591\text{-}2238}$	pET-*6HIS-SUMO-TgPDE2*$^{1591\text{-}2238}$ driven by a *T7* promoter with a *KanR* drug selectable marker.	Expression and purification of recombinant TgPDE2$^{1591\text{-}2238}$ from *E. coli*.	This work
p24	pET-*6HIS-SUMO-TgPDE3*$^{559\text{-}820}$	pET-*6HIS-SUMO-TgPDE3*$^{559\text{-}820}$ driven by a *T7* promoter with a *KanR* drug selectable marker.	Expression and purification of recombinant TgPDE3$^{559\text{-}820}$ from *E. coli*.	This work
p25	pET-*6HIS-SUMO-TgPDE4*$^{580\text{-}1033}$	pET-*6HIS-SUMO-TgPDE4*$^{580\text{-}1033}$ driven by a *T7* promoter with a *KanR* drug selectable marker.	Expression and purification of recombinant TgPDE4$^{580\text{-}1033}$ from *E. coli*.	This work
p26	pET-*6HIS-SUMO-TgPDE5*$^{721\text{-}1023}$	pET-*6HIS-SUMO-TgPDE5*$^{721\text{-}1023}$ driven by a *T7* promoter with a *KanR* drug selectable marker.	Expression and purification of recombinant TgPDE5$^{721\text{-}1023}$ from *E. coli*.	This work
p27	pET-*6HIS-SUMO-TgPDE6*$^{447\text{-}1065}$	pET-*6HIS-SUMO-TgPDE6*$^{447\text{-}1065}$ driven by a *T7* promoter with a KanR drug selectable marker.	Expression and purification of recombinant TgPDE6$^{447\text{-}1065}$ from *E. coli*.	This work
p28	pET-*6HIS-SUMO-TgPDE7*$^{675\text{-}1085}$	pET-*6HIS-SUMO-TgPDE7*$^{675\text{-}1085}$ driven by a *T7* promoter with a *KanR* drug selectable marker.	Expression and purification of recombinant TgPDE7$^{675\text{-}1085}$ from *E. coli*.	This work
p29	pET-*6HIS-SUMO-TgPDE8*$^{522\text{-}1123}$	pET-*6HIS-SUMO-TgPDE8*$^{522\text{-}1123}$ driven by a *T7* promoter with a *KanR* drug selectable marker.	Expression and purification of recombinant TgPDE8$^{522\text{-}1123}$ from *E. coli*.	This work
p30	pET-*6HIS-SUMO-TgPDE9*$^{650\text{-}1281}$	pET-*6HIS-SUMO-TgPDE9*$^{650\text{-}1281}$ driven by a *T7* promoter with a *KanR* drug selectable marker.	Expression and purification of recombinant TgPDE9$^{650\text{-}1281}$ from *E. coli*.	This work
p31	pET-*6HIS-SUMO-TgPDE10*$^{814\text{-}1294}$	pET-*6HIS-SUMO-TgPDE10*$^{814\text{-}1294}$ driven by a *T7* promoter with a *KanR* drug selectable marker.	Expression and purification of recombinant TgPDE10$^{814\text{-}1294}$ from *E. coli*.	This work
p32	pET-*6HIS-SUMO-TgPDE11*$^{540\text{-}1324}$	pET-*6HIS-SUMO-TgPDE11*$^{540\text{-}1324}$ driven by a *T7* promoter with a *KanR* drug selectable marker.	Expression and purification of recombinant TgPDE11$^{540\text{-}1324}$ from *E. coli*.	This work

p#	Plasmid Name	Description	Usage	Source
p33	pET-*6HIS-SUMO-TgPDE12*$^{1112-1579}$	pET-*6HIS-SUMO-TgPDE12*$^{1112-1579}$ driven by a *T7* promoter with a *KanR* drug selectable marker.	Expression and purification of recombinant TgPDE12$^{1112-1579}$ from *E. coli*.	This work
p34	pET-*6HIS-SUMO-TgPDE13*$^{1057-1656}$	pET-*6HIS-SUMO-TgPDE13*$^{1057-1656}$ driven by a *T7* promoter with a *KanR* drug selectable marker.	Expression and purification of recombinant TgPDE13$^{1057-1656}$ from *E. coli*.	This work
p35	pET-*6HIS-SUMO-TgPDE14*$^{6-291}$	pET-*6HIS-SUMO-TgPDE14*$^{6-291}$ driven by a *T7* promoter with a *KanR* drug selectable marker.	Expression and purification of recombinant TgPDE14$^{6-291}$ from *E. coli*.	This work
p36	pET-*6HIS-SUMO-TgPDE15*$^{952-1731}$	pET-*6HIS-SUMO-TgPDE15*$^{952-1731}$ driven by a *T7* promoter with a *KanR* drug selectable marker.	Expression and purification of recombinant TgPDE15$^{952-1731}$ from *E. coli*.	This work
p37	pET-*6HIS-SUMO-TgPDE16*$^{233-609}$	pET-*6HIS-SUMO-TgPDE16*$^{233-609}$ driven by a *T7* promoter with a *KanR* drug selectable marker.	Expression and purification of recombinant TgPDE16$^{233-609}$ from *E. coli*.	This work
p38	pET-*6HIS-SUMO-TgPDE17*$^{1405-1865}$	pET-*6HIS-SUMO-TgPDE17*$^{1405-1865}$ driven by a *T7* promoter with a *KanR* drug selectable marker.	Expression and purification of recombinant TgPDE17$^{1405-1865}$ from *E. coli*.	This work
p39	pET-*6HIS-SUMO-TgPDE18*$^{2700-3066}$	pET-*6HIS-SUMO-TgPDE18*$^{2700-3066}$ driven by a *T7* promoter with a *KanR* drug selectable marker.	Expression and purification of recombinant TgPDE18$^{2700-3066}$ from *E. coli*.	This work
p40	pET-*6HIS-SUMO-PfPDEα*$^{540-954}$	pET-*6HIS-SUMO-PfPDEα*$^{540-954}$ driven by a *T7* promoter with a *KanR* drug selectable marker.	Expression and purification of recombinant PfPDEα$^{540-954}$ from *E. coli*.	This work
p41	pET-*6HIS-SUMO-PfPDEβ*$^{688-1139}$	pET-*6HIS-SUMO-PfPDEβ*$^{688-1139}$ driven by a *T7* promoter with a *KanR* drug selectable marker.	Expression and purification of recombinant PfPDEβ$^{688-1139}$ from *E. coli*.	This work

Table S3 Oligonucleotides used in this study.

P#	ssDNA OligoNT Name	Sequence (5' – 3')	Usage	Source
P1	sg202540(PDE1) 3'UTR	TAAATGGGGATGTCAAGTTGAGGAGAGAAG CGCCGCTCTGTTTTAGAGCTAGAAATAGC	HiFi assembly of p*SAG1:Cas9-GFP, U6:sg202540(PDE1) 3'UTR*	This work; IDT
P2	sg293000(PDE2) 3'UTR	TAAATGGGGATGTCAAGTTgAGACGCCAAG GAACGGCGCAGTTTTAGAGCTAGAAATAGC	HiFi assembly of p*SAG1:Cas9-GFP, U6:sg293000(PDE2) 3'UTR*	This work; IDT
P3	sg233065(PDE3) 3'UTR	TAAATGGGGATGTCAAGTTgACCTGCTGAA GTAGAAGAAGGTTTTAGAGCTAGAAATAGC	HiFi assembly of p*SAG1:Cas9-GFP, U6:sg233065(PDE3) 3'UTR*	This work; IDT
P4	sg229405(PDE4) 3'UTR	TAAATGGGGATGTCAAGTTgTCACGAATCT TCCACACCATGTTTTAGAGCTAGAAATAGC	HiFi assembly of p*SAG1:Cas9-GFP, U6:sg229405(PDE4) 3'UTR*	This work; IDT
P5	sg220420(PDE5) 3'UTR	TAAATGGGGATGTCAAGTTgCGCGAAGGCT TCAACGCCTGGTTTTAGAGCTAGAAATAGC	HiFi assembly of p*SAG1:Cas9-GFP, U6:sg220420(PDE5) 3'UTR*	This work; IDT
P6	sg266920(PDE6) 3'UTR	TAAATGGGGATGTCAAGTTgTGAAGCCACC TGTTCTTCGTGTTTTAGAGCTAGAAATAGC	HiFi assembly of p*SAG1:Cas9-GFP, U6:sg266920(PDE6) 3'UTR*	This work; IDT
P7	sg280410(PDE7) 3'UTR	TAAATGGGGATGTCAAGTTGTAAAGCAGTG CCCTGAGAAGTTTTAGAGCTAGAAATAGC	HiFi assembly of p*SAG1:Cas9-GFP, U6:sg280410(PDE7) 3'UTR*	This work; IDT
P8	sg318675(PDE8) 3'UTR	TAAATGGGGATGTCAAGTTgCGAGCCAAAG GACAAAGTTGGTTTTAGAGCTAGAAATAGC	HiFi assembly of p*SAG1:Cas9-GFP, U6:sg318675(PDE8) 3'UTR*	This work; IDT
P9	sg241880(PDE9) 3'UTR	TAAATGGGGATGTCAAGTTgAGCGAGGAGC TGGAACGTCGGTTTTAGAGCTAGAAATAGC	HiFi assembly of p*SAG1:Cas9-GFP, U6:sg241880(PDE9) 3'UTR*	This work; IDT
P10	sg272650(PDE10) 3'UTR	TAAATGGGGATGTCAAGTTGAGATGAACCA TGACACTCGGTTTTAGAGCTAGAAATAGC	HiFi assembly of p*SAG1:Cas9-GFP, U6:sg272650(PDE10) 3'UTR*	This work; IDT
P11	sg224840(PDE11) 3'UTR	TAAATGGGGATGTCAAGTTGAGAATGTGCA AAACAATTCGTTTTAGAGCTAGAAATAGC	HiFi assembly of p*SAG1:Cas9-GFP, U6:sg224840(PDE11) 3'UTR*	This work; IDT
P12	sg310520(PDE12) 3'UTR	TAAATGGGGATGTCAAGTTgCATCTAAAAA CATCGCACACGTTTTAGAGCTAGAAATAGC	HiFi assembly of p*SAG1:Cas9-GFP, U6:sg310520(PDE12) 3'UTR*	This work; IDT
P13	sg257080(PDE13) 3'UTR	TAAATGGGGATGTCAAGTTGAGAGCCAAAA GCGCTTTCAGTTTTAGAGCTAGAAATAGC	HiFi assembly of p*SAG1:Cas9-GFP, U6:sg257080(PDE13) 3'UTR*	This work; IDT
P14	sg228500(PDE14) 3'UTR	TAAATGGGGATGTCAAGTTgAGACCACCGA GTCAGCTAGGGTTTTAGAGCTAGAAATAGC	HiFi assembly of p*SAG1:Cas9-GFP, U6:sg228500(PDE14) 3'UTR*	This work; IDT
P15	sg233040(PDE15) 3'UTR	TAAATGGGGATGTCAAGTTgCCTGAAATGG TATTACGAAGGTTTTAGAGCTAGAAATAGC	HiFi assembly of p*SAG1:Cas9-GFP, U6:sg233040(PDE15) 3'UTR*	This work; IDT
P16	sg258508(PDE16) 3'UTR	TAAATGGGGATGTCAAGTTgCTTTGGAACG ACTACAGTATGTTTTAGAGCTAGAAATAGC	HiFi assembly of p*SAG1:Cas9-GFP, U6:sg258508(PDE16) 3'UTR*	This work; IDT
P17	sg257945(PDE17) 3'UTR	TAAATGGGGATGTCAAGTTgTTCTGGTGCC CCTCCTCAGCGTTTTAGAGCTAGAAATAGC	HiFi assembly of p*SAG1:Cas9-GFP, U6:sg257945(PDE17) 3'UTR*	This work; IDT
P18	sg226755(PDE18) 3'UTR	TAAATGGGGATGTCAAGTTgAGAACGAAGC AGATTGACAAGTTTTAGAGCTAGAAATAGC	HiFi assembly of p*SAG1:Cas9-GFP, U6:sg226755(PDE18) 3'UTR*	This work; IDT
P19	pU6_Seq_F	CTCTCGAATGTCTTCTCTGACAAG	Sanger sequencing primer for p*SAG1:Cas9-GFP, U6:sg"GOI" 3' UTR*	This work; IDT
P20	tag202540(PDE1) F	CCAACAAAGTGGAAGAAGAGTATCTGAAGG CACATCCGCCGCTAGCAAGGGCTCGGGCTC	Amplify *TgPDE1-mAID-3HA, DHFR-TS:HXGPRT* tagging amplicon from p*TUB1:YFP-mAID-3HA, DHFR-TS:HXGPRT*	This work; IDT
P21	tag202540(PDE1) R	TAGATAGATCGATAGATCGATGGATCGTTT GAGGTCTGCTATAGGGCGAATTGGAGCTCC		This work; IDT
P22	tag293000(PDE2) F	CGAGGAGTTCGACGGCTATCGACCGCCCAG CTTGGACGTAGCTAGCAAGGGCTCGGGCTC	Amplify *TgPDE2-mAID-3HA, DHFR-TS:HXGPRT* tagging amplicon from p*TUB1:YFP-mAID-3HA, DHFR-TS:HXGPRT*	This work; IDT
P23	tag293000(PDE2) R	CCATCTGCCATTCTTCTTTCTCGTTGACGC GCTCCGACCTATAGGGCGAATTGGAGCTCC		This work; IDT
P24	tag233065(PDE3) F	AAACAAATGGAAATCCATCATCGATGGGCA TGAACGTCGGGCTAGCAAGGGCTCGGGCTC	Amplify *TgPDE3-mAID-3HA, DHFR-TS:HXGPRT* tagging amplicon from p*TUB1:YFP-mAID-3HA, DHFR-TS:HXGPRT*	This work; IDT
P25	tag233065(PDE3) R	GGTCGAAAGGAGTCTCTCTGTGTCAGAATC TTTGTTCAGAATAGGGCGAATTGGAGCTCC		This work; IDT
P26	tag229405(PDE4) F	GGAGCTCCGGGCCAACGCGAATCCATTATC GGAGGTCGACGCTAGCAAGGGCTCGGGCTC	Amplify *TgPDE4-mAID-3HA, DHFR-TS:HXGPRT* tagging amplicon from p*TUB1:YFP-mAID-3HA, DHFR-TS:HXGPRT*	This work; IDT
P27	tag229405(PDE4) R	GGTCGTCCTCCGGTCAAGACCAGTTTTCCG GTACATCCCGATAGGGCGAATTGGAGCTCC		This work; IDT
P28	tag220420(PDE5) F	GAACTCTGCTGAGGCCCTGCAGGAAGGATT TAAAACGGTCGCTAGCAAGGGCTCGGGCTC	Amplify *TgPDE5-mAID-3HA, DHFR-TS:HXGPRT* tagging amplicon from	This work; IDT

P#	ssDNA OligoNT Name	Sequence (5' – 3')	Usage	Source
P29	tag220420(PDE5) R	AAAAATACAAAAGCATTCTCGGAGGGCGCA AGGGACACCAATAGGGCGAATTGGAGCTCC	p*TUB1:YFP-mAID-3HA, DHFR-TS:HXGPRT*	This work; IDT
P30	tag266920(PDE6) F	CAACACTCCGTGTGGTGGCGAGGCAAACAC CTTGGAGTCGGCTAGCAAGGGCTCGGGCTC	Amplify *TgPDE6-mAID-3HA, DHFR-TS:HXGPRT* tagging amplicon from p*TUB1:YFP-mAID-3HA, DHFR-TS:HXGPRT*	This work; IDT
P31	tag266920(PDE6) R	AACACCCGTAACACAGATGCACTCCCATAA AGCTGCTTTTATAGGGCGAATTGGAGCTCC		This work; IDT
P32	tag280410(PDE7) F	GGCTTCTCTGGAACCGGCTGGTCTAGAAGT TGGAGGAGCGGCTAGCAAGGGCTCGGGCTC	Amplify *TgPDE7-mAID-3HA, DHFR-TS:HXGPRT* tagging amplicon from p*TUB1:YFP-mAID-3HA, DHFR-TS:HXGPRT*	This work; IDT
P33	tag280410(PDE7) R	TAATCCGGCTGTCTGTCTCTTCTCTCTTGG GTCTGAACCGATAGGGCGAATTGGAGCTCC		This work; IDT
P34	tag318675(PDE8) F	TTTTACATCGAATAGTCTTTTCGATGGGCT TAATCGGTCCGCTAGCAAGGGCTCGGGCTC	Amplify *TgPDE8-mAID-3HA, DHFR-TS:HXGPRT* tagging amplicon from p*TUB1:YFP-mAID-3HA, DHFR-TS:HXGPRT*	This work; IDT
P35	tag318675(PDE8) R	ACCAGAAGAATTCACGGCCGTCGCTCGACA GCAGGCACCGATAGGGCGAATTGGAGCTCC		This work; IDT
P36	tag241880(PDE9) F	CAGGAAGGACCTTCTCCATTTCGAATCGCG ACTGACGCATGCTAGCAAGGGCTCGGGCTC	Amplify *TgPDE9-mAID-3HA, DHFR-TS:HXGPRT* tagging amplicon from p*TUB1:YFP-mAID-3HA, DHFR-TS:HXGPRT*	This work; IDT
P37	tag241880(PDE9) R	TTCTCCCGACCGTTTTTCAACAAGATCAGC ATGTCTTCCTATAGGGCGAATTGGAGCTCC		This work; IDT
P38	tag272650(PDE10) F	GGAAGGGGCGCAAGACGAAGTCGACCAGGC AAGCGCAAAGGCTAGCAAGGGCTCGGGCTC	Amplify *TgPDE10-mAID-3HA, DHFR-TS:HXGPRT* tagging amplicon from p*TUB1:YFP-mAID-3HA, DHFR-TS:HXGPRT*	This work; IDT
P39	tag272650(PDE10) R	GACTTCAACACGCAGACGTCCTCTCTACCT CTTCCTCCCTATAGGGCGAATTGGAGCTCC		This work; IDT
P40	tag224840(PDE11) F	GACGATGAAGAATCCAGAACACCACGCGTC TCAGAAGCAAGCTAGCAAGGGCTCGGGCTC	Amplify *TgPDE11-mAID-3HA, DHFR-TS:HXGPRT* tagging amplicon from p*TUB1:YFP-mAID-3HA, DHFR-TS:HXGPRT*	This work; IDT
P41	tag224840(PDE11) R	ACGGAACGAGAAATGTCAAAGTCAGGGCCA AGGAGGCCGCATAGGGCGAATTGGAGCTCC		This work; IDT
P42	tag310520(PDE12) F	AAGTGCCTGCGAGTCCCTTAGAGTGGGGCC GCGGGAAGTGGCTAGCAAGGGCTCGGGCTC	Amplify *TgPDE12-mAID-3HA, DHFR-TS:HXGPRT* tagging amplicon from p*TUB1:YFP-mAID-3HA, DHFR-TS:HXGPRT*	This work; IDT
P43	tag310520(PDE12) R	TTCGGCGGACTACGTCTGTGCAAATGTCCT GCACCTGCCAATAGGGCGAATTGGAGCTCC		This work; IDT
P44	tag257080(PDE13) F	GAAGCGTCGCGACGAGAAGAAGCCCGAGAA GAGCAAGACAGCTAGCAAGGGCTCGGGCTC	Amplify *TgPDE13-mAID-3HA, DHFR-TS:HXGPRT* tagging amplicon from p*TUB1:YFP-mAID-3HA, DHFR-TS:HXGPRT*	This work; IDT
P45	tag257080(PDE13) R	ATGCCGCATTCCCGCAAATGGCTGTTGGTA GATCTGTCCCATAGGGCGAATTGGAGCTCC		This work; IDT
P46	tag228500(PDE14) F	GCAGAAAAACAGGTGTGTACCTTTGATTAT CTTCCCCACCGCTAGCAAGGGCTCGGGCTC	Amplify *TgPDE14-mAID-3HA, DHFR-TS:HXGPRT* tagging amplicon from p*TUB1:YFP-mAID-3HA, DHFR-TS:HXGPRT*	This work; IDT
P47	tag228500(PDE14) R	AGCTATGTGGGCGCCAAGAAACTCGAAGGT CAGGAGTATTATAGGGCGAATTGGAGCTCC		This work; IDT
P48	tag233040(PDE15) F	TCAAGATCAAGAACAAGCGGACTATGCGTA TCCAGAAGGTGCTAGCAAGGGCTCGGGCTC	Amplify *TgPDE15-mAID-3HA, DHFR-TS:HXGPRT* tagging amplicon from p*TUB1:YFP-mAID-3HA, DHFR-TS:HXGPRT*	This work; IDT
P49	tag233040(PDE15) R	TGGAACTATCACACACAGTTAACTCAATAC CCGTCATCCTATAGGGCGAATTGGAGCTCC		This work; IDT
P50	tag258508(PDE16) F	AAATCAGAAGAACCTCATGCAAAAACTGGA CAAAAGTGATGCTAGCAAGGGCTCGGGCTC	Amplify *TgPDE16-mAID-3HA, DHFR-TS:HXGPRT* tagging amplicon from p*TUB1:YFP-mAID-3HA, DHFR-TS:HXGPRT*	This work; IDT
P51	tag258508(PDE16) R	AATTTGTAAACATTGAAGCGGTGGATATTC ACACATCCCGATAGGGCGAATTGGAGCTCC		This work; IDT
P52	tag257945(PDE17) F	CCGGAGGCACCTCAAACGATGGTCAACGAT CTCACCCTGCGCTAGCAAGGGCTCGGGCTC	Amplify *TgPDE17-mAID-3HA, DHFR-TS:HXGPRT* tagging amplicon from p*TUB1:YFP-mAID-3HA, DHFR-TS:HXGPRT*	This work; IDT
P53	tag257945(PDE17) R	ACGGCTGACGGTAAATTCTTGGGCGTGTGC GCTGCTCTTTATAGGGCGAATTGGAGCTCC		This work; IDT
P54	tag226755(PDE18) F	GGAACTGTTGCACGTCGAAAAAAGGGTGTG CGAAACAGTGGCTAGCAAGGGCTCGGGCTC	Amplify *TgPDE18-mAID-3HA, DHFR-TS:HXGPRT* tagging amplicon from p*TUB1:YFP-mAID-3HA, DHFR-TS:HXGPRT*	This work; IDT
P55	tag226755(PDE18) R	CCCTCAGTCCTCCTTGTTTCTTATCCTTCA CAATCGCCCTATAGGGCGAATTGGAGCTCC		This work; IDT
P56	202540(PDE1)_3' F	CCGCAGAAATCGCAAACAG	Forward primer for *TgPDE1* Diagnostic PCRs 1, 2	This work; IDT
P57	202540(PDE1)_3' R	TGTGTATGTAACAACGGACATAGA	Reverse primer for *TgPDE1* Diagnostic PCR 1	This work; IDT

P#	ssDNA OligoNT Name	Sequence (5' – 3')	Usage	Source
P58	293000(PDE2)_3' F	GGGTTCCTACGTCTTTCTTTCA	Forward primer for *TgPDE2* Diagnostic PCRs 1, 2	This work; IDT
P59	293000(PDE2)_3' R	CTGAATGCGGAACGCAAATC	Reverse primer for *TgPDE2* Diagnostic PCR 1	This work; IDT
P60	233065(PDE3)_3' F	TGCTGCACATTTGAGCGT	Forward primer for *TgPDE3* Diagnostic PCRs 1, 2	This work; IDT
P61	233065(PDE3)_3' R	CGACCCGCTAAGAAATTCATGT	Reverse primer for *TgPDE3* Diagnostic PCR 1	This work; IDT
P62	229405(PDE4)_3' F	CGACTGAGGCAACAGGAAA	Forward primer for *TgPDE4* Diagnostic PCRs 1, 2	This work; IDT
P63	229405(PDE4)_3' R	GAGATGTTCCGCCCATGAA	Reverse primer for *TgPDE4* Diagnostic PCR 1	This work; IDT
P64	220420(PDE5)_3' F	CCTCCGTTCTTCATTCCTTGT	Forward primer for *TgPDE5* Diagnostic PCRs 1, 2	This work; IDT
P65	220420(PDE5)_3' R	GTAACTCAGGAGAAAGCGTACC	Reverse primer for *TgPDE5* Diagnostic PCR 1	This work; IDT
P66	266920(PDE6)_3' F	CTGCCCGTCTCTACTACAGAAT	Forward primer for *TgPDE6* Diagnostic PCRs 1, 2	This work; IDT
P67	266920(PDE6)_3' R	CGCTGCGTACCAAACCTTTA	Reverse primer for *TgPDE6* Diagnostic PCR 1	This work; IDT
P68	280410(PDE7)_3' F	TAAACCCTCAGCTGCCAATC	Forward primer for *TgPDE7* Diagnostic PCRs 1, 2	This work; IDT
P69	280410(PDE7)_3' R	TATCTCAGCTTCTCGCCTCT	Reverse primer for *TgPDE7* Diagnostic PCR 1	This work; IDT
P70	318675(PDE8)_3' F	GAGGGACACGACAATGAGAAG	Forward primer for *TgPDE8* Diagnostic PCRs 1, 2	This work; IDT
P71	318675(PDE8)_3' R	TGCCTGTTTCCTGACATACTG	Reverse primer for *TgPDE8* Diagnostic PCR 1	This work; IDT
P72	241880(PDE9)_3' F	CACGAGAGGAACAGACAAGAC	Forward primer for *TgPDE9* Diagnostic PCRs 1, 2	This work; IDT
P73	241880(PDE9)_3' R	GATACCGAGACATCTTCCTCAAC	Reverse primer for *TgPDE9* Diagnostic PCR 1	This work; IDT
P74	272650(PDE10)_3' F	CTCTCGCGCAACACCTC	Forward primer for *TgPDE10* Diagnostic PCRs 1, 2	This work; IDT
P75	272650(PDE10)_3' R	CTGCAGGCCAGTCTTCTG	Reverse primer for *TgPDE10* Diagnostic PCR 1	This work; IDT
P76	224840(PDE11)_3' F	CTGAATTGGTGCATGGTTTCTT	Forward primer for *TgPDE11* Diagnostic PCRs 1, 2	This work; IDT
P77	224840(PDE11)_3' R	TCTGTCACGAACCTAGGACT	Reverse primer for *TgPDE11* Diagnostic PCR 1	This work; IDT
P78	310520(PDE12)_3' F	TTCTCGATTACGGAGGCTAC	Forward primer for *TgPDE12* Diagnostic PCRs 1, 2	This work; IDT
P79	310520(PDE12)_3' R	AAACGTTCCTAGCATTGTGAG	Reverse primer for *TgPDE12* Diagnostic PCR 1	This work; IDT
P80	257080(PDE13)_3' F	CGCAGACGAAGCAGGATT	Forward primer for *TgPDE13* Diagnostic PCRs 1, 2	This work; IDT
P81	257080(PDE13)_3' R	ACGACAACTTGAGTGACAGTG	Reverse primer for *TgPDE13* Diagnostic PCR 1	This work; IDT
P82	228500(PDE14)_3' F	TTGCCTTTATGTGTTGCAGATG	Forward primer for *TgPDE14* Diagnostic PCRs 1, 2	This work; IDT
P83	228500(PDE14)_3' R	CTACGGCCTTGCGATCATTA	Reverse primer for *TgPDE14* Diagnostic PCR 1	This work; IDT
P84	233040(PDE15)_3' F	GGAGCTTTCCAGGCGTATT	Forward primer for *TgPDE15* Diagnostic PCRs 1, 2	This work; IDT
P85	233040(PDE15)_3' R	AAATGCATACCGCCCTTACA	Reverse primer for *TgPDE15* Diagnostic PCR 1	This work; IDT
P86	258508(PDE16)_3' F	AGCCACTGATGACGGTTT	Forward primer for *TgPDE16* Diagnostic PCRs 1, 2	This work; IDT

P#	ssDNA OligoNT Name	Sequence (5' – 3')	Usage	Source
P87	258508(PDE16)_3' R	GATACAACACAACACTTGATCCC	Reverse primer for *TgPDE16* Diagnostic PCR 1	This work; IDT
P88	257945(PDE17)_3' F	CCATGGCCGAGGAACAG	Forward primer for *TgPDE17* Diagnostic PCRs 1, 2	This work; IDT
P89	257945(PDE17)_3' R	CATAAGAGTGGAACGGAGAAGG	Reverse primer for *TgPDE17* Diagnostic PCR 1	This work; IDT
P90	226755(PDE18)_3' F	GCGAGAAGCCAGTAAAGAGAA	Forward primer for *TgPDE18* Diagnostic PCRs 1, 2	This work; IDT
P91	226755(PDE18)_3' R	GTGCAGCTTTGACGCATAAC	Reverse primer for *TgPDE18* Diagnostic PCR 1	This work; IDT
P92	HXG 3' UTR R	GCTATTATACCCGTGTGTTACG	Reverse primer for all *TgPDE* Diagnostic PCR 2	This work; IDT
P93	pET-SUMO F	TAGAGACAAGCTTAGGTATTTATTCGGCG	Amplify vector backbone from pET-*6HIS-SUMO-hGSDMD* plasmid	This work; IDT
P94	pET-SUMO R	ACCACCAATCTGTTCTCTGTGAG		This work; IDT
P95	SUMO Seq F	CTGAAGATTTGGACATGGAGG	Sanger sequencing primers for confirmation of *TgPDE* plasmid sequences	This work; IDT
P96	SUMO Seq R	GCATCACCCGACGCACTTTG		This work; IDT
P97	202540(PDE1) CAT F	ACAGAGAACAGATTGGTGGTTGCCACCAAACGCTGAGTC	Amplify sequence corresponding to TgPDE1$^{974-1670}$ from RH cDNA with homology flanks to pET-*6HIS-SUMO* plasmid for HiFi assembly	This work; IDT
P98	202540(PDE1) CAT R	AATACCTAAGCTTGTCTCTAGGCGGATGTGCCTTCAGAT		This work; IDT
P99	293000(PDE2) CAT F	ACAGAGAACAGATTGGTGGTTTGCTAGCAACGCGTCTGTC	Amplify sequence corresponding to TgPDE2$^{1591-2238}$ from RH cDNA with homology flanks to pET-*6HIS-SUMO* plasmid for HiFi assembly	This work; IDT
P100	293000(PDE2) CAT R	AATACCTAAGCTTGTCTCTATACGTCCAAGCTGGGCGGTCGATAGCC		This work; IDT
P101	233065(PDE3) CAT F	ACAGAGAACAGATTGGTGGTGGCTTTGCCGTTGCTCTCTAT	Amplify sequence corresponding to TgPDE3$^{559-820}$ from RH cDNA with homology flanks to pET-*6HIS-SUMO* plasmid for HiFi assembly	This work; IDT
P102	233065(PDE3) CAT R	AATACCTAAGCTTGTCTCTATTTCCATTTGTTTCTGTTCTTTCG		This work; IDT
P103	229405(PDE4) CAT F	ACAGAGAACAGATTGGTGGTCTCTACGAGATGGGATCGGAA	Amplify sequence corresponding to TgPDE4$^{580-1033}$ from RH cDNA with homology flanks to pET-*6HIS-SUMO* plasmid for HiFi assembly	This work; IDT
P104	229405(PDE4) CAT R	AATACCTAAGCTTGTCTCTATAATGGATTCGCGTTGGCCC		This work; IDT
P105	220420(PDE5) CAT F	ACAGAGAACAGATTGGTGGTTGGCGTAACTTCCTCAGAGAAG	Amplify sequence corresponding to TgPDE5$^{721-1023}$ from RH cDNA with homology flanks to pET-*6HIS-SUMO* plasmid for HiFi assembly	This work; IDT
P106	220420(PDE5) CAT R	AATACCTAAGCTTGTCTCTATTTCGTCTTTATTCGGTTCCAGG		This work; IDT
P107	266920(PDE6) CAT F	ACAGAGAACAGATTGGTGGTGGGATCCTCGTGAATGAGCT	Amplify sequence corresponding to TgPDE6$^{447-1065}$ from RH cDNA with homology flanks to pET-*6HIS-SUMO* plasmid for HiFi assembly	This work; IDT
P108	266920(PDE6) CAT R	AATACCTAAGCTTGTCTCTACGACTCCAAGGTGTTTGCC		This work; IDT
P109	280410(PDE7) CAT F	ACAGAGAACAGATTGGTGGTATTTTCGCGTTGATGCAGGA	Amplify sequence corresponding to TgPDE7$^{675-1085}$ from RH cDNA with homology flanks to pET-*6HIS-SUMO* plasmid for HiFi assembly	This work; IDT
P110	280410(PDE7) CAT R	AATACCTAAGCTTGTCTCTACGCTCCTCCAACTTCTAGACC		This work; IDT
P111	318675(PDE8) CAT F	ACAGAGAACAGATTGGTGGTGCTCTCGAGCTTGTAGAGGAAG	Amplify sequence corresponding to TgPDE8$^{522-1123}$ from RH cDNA with homology flanks to pET-*6HIS-SUMO* plasmid for HiFi assembly	This work; IDT
P112	318675(PDE8) CAT R	AATACCTAAGCTTGTCTCTAGGACCGATTAAGCCCATCGA		This work; IDT
P113	241880(PDE9) CAT F	ACAGAGAACAGATTGGTGGTTCTGAGGGCATGCTTATCAGG	Amplify sequence corresponding to TgPDE9$^{650-1281}$ from RH cDNA with homology flanks to pET-*6HIS-SUMO* plasmid for HiFi assembly	This work; IDT
P114	241880(PDE9) CAT R	AATACCTAAGCTTGTCTCTAATGCGTCAGTCGCGATTC		This work; IDT
P115	272650(PDE10) CAT F	ACAGAGAACAGATTGGTGGTCTGGATGCCCTCCGAGTC	Amplify sequence corresponding to TgPDE10$^{814-1294}$ from RH cDNA with	This work; IDT

P#	ssDNA OligoNT Name	Sequence (5' – 3')	Usage	Source
P116	272650(PDE10) CAT R	AATACCTAAGCTTGTCTCTACTTTGCGCTTGCCTGGTC	homology flanks to pET-*6HIS-SUMO* plasmid for HiFi assembly	This work; IDT
P117	224840(PDE11) CAT F	ACAGAGAACAGATTGGTGGTGAGAAGCTTCTCGAAAGAATCCTTG	Amplify sequence corresponding to TgPDE11$^{540-1324}$ from RH cDNA with homology flanks to pET-*6HIS-SUMO* plasmid for HiFi assembly	This work; IDT
P118	224840(PDE11) CAT R	AATACCTAAGCTTGTCTCTATTGCTTCTGAGACGCGTG		This work; IDT
P119	310520(PDE12) CAT F	ACAGAGAACAGATTGGTGGTAGTAGGGGGAAGCGAGAGGAAGAGC	Amplify sequence corresponding to TgPDE12$^{1112-1579}$ from RH cDNA with homology flanks to pET-*6HIS-SUMO* plasmid for HiFi assembly	This work; IDT
P120	310520(PDE12) CAT R	AATACCTAAGCTTGTCTCTACACTTCCCGCGGCCCCAC		This work; IDT
P121	257080(PDE13) CAT F	ACAGAGAACAGATTGGTGGTGTGGCTGACATTCAAGGACAA	Amplify sequence corresponding to TgPDE13$^{1057-1656}$ from RH cDNA with homology flanks to pET-*6HIS-SUMO-hGSDMD* plasmid for HiFi assembly	This work; IDT
P122	257080(PDE13) CAT R	AATACCTAAGCTTGTCTCTATGTCTTGCTCTTCTCGGGC		This work; IDT
P123	228500(PDE14) CAT F	ACAGAGAACAGATTGGTGGTGACTGGGATTTTCACGTCCT	Amplify sequence corresponding to TgPDE14$^{6-291}$ from RH cDNA with homology flanks to pET-*6HIS-SUMO* plasmid for HiFi assembly	This work; IDT
P124	228500(PDE14) CAT R	AATACCTAAGCTTGTCTCTACAGCTGGGCAGGAAACATGA		This work; IDT
P125	233040(PDE15) CAT F	ACAGAGAACAGATTGGTGGTGAGCCTGCAGGCCAGGAA	Amplify sequence corresponding to TgPDE15$^{952-1731}$ from RH cDNA with homology flanks to pET-*6HIS-SUMO* plasmid for HiFi assembly	This work; IDT
P126	233040(PDE15) CAT R	AATACCTAAGCTTGTCTCTAACCTTCTGGATACGCATAGTCCGC		This work; IDT
P127	258508(PDE16) CAT F	ACAGAGAACAGATTGGTGGTACTGCGACCGTTGGAGGTATG	Amplify sequence corresponding to TgPDE16$^{233-609}$ from RH cDNA with homology flanks to pET-*6HIS-SUMO* plasmid for HiFi assembly	This work; IDT
P128	258508(PDE16) CAT R	AATACCTAAGCTTGTCTCTAATCACTTTTGTCCAGTTTTTGCATG		This work; IDT
P129	257945(PDE17) CAT F	ACAGAGAACAGATTGGTGGTCACCGTCGGCCCTCTCTAAGTG	Amplify sequence corresponding to TgPDE17$^{1405-1865}$ from RH cDNA with homology flanks to pET-*6HIS-SUMO* plasmid for HiFi assembly	This work; IDT
P130	257945(PDE17) CAT R	AATACCTAAGCTTGTCTCTAGGATGCTTCGAAGTTTCTGCC		This work; IDT
P131	226755(PDE18) CAT F	ACAGAGAACAGATTGGTGGTGAGCACGTGCACTCGAGCC	Amplify sequence corresponding to TgPDE18$^{2700-3066}$ from RH cDNA with homology flanks to pET-*6HIS-SUMO* plasmid for HiFi assembly	This work; IDT
P132	226755(PDE18) CAT R	AATACCTAAGCTTGTCTCTAATCGGAAGAACTAAACGCTTTACTC		This work; IDT
P133	1209500(PfPDEα) CAT F	ACAGAGAACAGATTGGTGGTATCAAAGAAAAAATCAAAAATTGTGATAAT	Amplify sequence corresponding to PfPDEα$^{540-954}$ from *P. falciparum* cDNA with homology flanks to pET-*6HIS-SUMO* plasmid for HiFi assembly	This work; IDT
P134	1209500(PfPDEα) CAT R	AATACCTAAGCTTGTCTCTATTCAAATTTGATGAGCTCAAGT		This work; IDT
P135	1321500(PfPDEβ) CAT F	ACAGAGAACAGATTGGTGGTTGTTCGAATATTTTGGAACAATG	Amplify sequence corresponding to PfPDEβ$^{688-1139}$ from *P. falciparum* cDNA with homology flanks to pET-*6HIS-SUMO* plasmid for HiFi assembly	This work; IDT
P136	1321500(PfPDEβ) CAT R	AATACCTAAGCTTGTCTCTAATCGGAAACATTTTTTATAAAAAATAGAGT		This work; IDT

dsDNA OligoNT sequences continued on next page.

G#	dsDNA OligoNT (gBlock) Name	Sequence (5’ - 3’)	Usage	Source
G1	233065(PDE3) CAT gBlock	ACAGAGAACAGATTGGTGGTGGCTTTGCCGTTGCTCTCTATAAAAACTACGAACAGA ATCCGTACCACAATTTCTTTCATGCCCTCAATGTCGCCCAAGTCTGCTGCCTGCTCA TGGCCCTGCCAGACGTCGCGGCTCGGTTCCAACCTCTGGACTACTTTGTGCTCTCCG TCGCTGCTTTGGGCCATGACCTAGGCCACCCAGGCGCGAACAATCTCTTCGTCAATC GAAACGACTGCTTGCCCTCTCGTCTCTACCAGAACCGGTCTGTTCTCGAAAACTACC ACGCGGCTCTACTTTTCCAAATTCTCCGGCACCCCCGGTTTAACGTATTCTGCTCCA TTCCGCCTCAAGCCTTCTCGGCTTGCCGACAGCGCATCATCAGCGCGATTCTGTGGA CCGACATGGCCAAGCATTTCGACATGGTCGCGCAACTCAAGGCGAAAATCGAGGACG AAATGGTGTTGACCGAAGGCATCATTGTCACGCTGCAAAAGCCGTATCTGGAGGGGC TGCTCCTCCACGCCTCCGACATTTCAAATCCCTTGCTCAGTTTCGATCTCTCCTTCG ACTGGGCTGTCAGAGCCTGCGACGAATTCTTTCAGCAGAACAAACTCGAAGAGAAGC TCGGCCAGCCGCCGCACATGCCTACCTTCGCGGCATTCGACCTCTACAACGTCGCAA AATGCCAAGTGAATTTCATAGATTTTATTTGTCGCCCCCTCTTCGGTAGCCTCGCGC AGATGTTCCCGGCCCAGCTTGGAGACCGAGCTGCGGAGCTCCGAAAGAACAGAAACA AATGGAAATAGAGACAAGCTTAGGTATT	Clone TgGT1_233065 catalytic domain (TgPDE3$^{559-820}$) into pET-*6HIS-SUMO* by HiFi assembly	This work; IDT
G2	233040(PDE15) CAT gBlock	ACAGAGAACAGATTGGTGGTGAGCCTGCAGGCCAGGAAGACGAACTCCCCACTGCTG AACGGACGACGGAGGAATTCAGATGGGGCAACATTCCCGAGTACACAGTGCCGAGCT GCATCACGGCGAGTGTTGCCAGGATGGATACAGTCTTGTGCTTGGCTCCGAGCATCG CGTCGGAGGCACGACTAAACACGTACAGAGAAAATGCTCCATCAATCGCTGTCGAGT TCATCTTCAGCTGGGACTTTGATATCTCCAGTCTCCAACCTGAAATGTCTGCGAAAC TGGCGTACGAGTTGCTGATTTGGTGTGCAGATAAAGCGCACATTAGCGTTCCTCGGG AGACGTGCGAGAAGTTCGTCCTCTCTGTGCAGCAGAACTATTCTGCAATGCCTTTCC ATAACTTCAACCACGCGTTGCATGCAGCTCAAGCAGTGATATTGATTGCAAAAGACC TGTCTTTTCAACATTGGTTTTCTTACGAAGATAAATTTATTATTATGCTCGCGGCGC TGGGTCATGACATGGGCCACCCTGGAGTATCAAATGAGTTTCTGATTAGCATGCGAT CGTTCACGAGCATCTTGTTCAACGAAACGGCCGTTCTGGAGAATTACCACACCTTGC TTTACATGGATCTTTTGAAAAACTCTGATCTGGACATTTTGAAAATGCTCCAGCCCG AGGCCGTCCAGCGGGCGCGACAGAGAATCATCGCAGCCATCTTGGCCACCGATCGCG CGTTAGACATGAAACTCATTGACCTTCTGAACGATGTCAAAAGCAAAAACGAGAAAG TGCCGGTACCCGCCGCGCTCCTCGATCCAAATGTCAGGGACGCCTGTCTCATTCATG CGGCTGACCACGCTCTCTCGCTGCTCAACTTTCCACTCCATCGGAAGTGGGCTGAGA AAATGGCGATCGAAATGCACTTCCAGAACACTATGGACGAAGCCTTAAAGCTGCCCA AGAGCTACTGCAGCCTCAGTAGATTAACAGAAGCATCCCTTGCTGGATCCCAAGTGA CGATGATAGATACACACTACCTGCCATTCTTCAGCGCCCTCGCTTGGTATTTCCCTG GCGACCTCGATATGAGAGTTGCTGTGATGAAAGCCAACGCTGCGTTCTGGCAGCATC TTCGTGATGAAGAAATGAGGAAAACAGTCGCACTGAATGACAATCCGGAGCAAGAAG ATTGGAGGAGTGCAAAACTGCAAGTAATCTCTAGCAAATTCGTCGAGAATAGAGAGA AAATGCACCAGAAAGCGGCGGAAATGATGCAGGCCGAGGCTACAGATGTTTTCTTTG ACCCTTACCCAATGATAGTAGATCAAAGTGGCAACGAGGGCGAAGAGGACTCCTTCG CGAAAGGGGTGATGCGCGAGAAATCCGGAATGGGGGGGTACGCAATAGAGAGCAGAC GTCGGTCAGCTGATTCATCCAGGGGAGCGGAACGGCGGGAATCAGATGCTGAAGCTC ATCATTCGGAAGCAACGCATGCCCCGAAACCAGACGAAAAGTCTCAGTTAGACAAGA ATGGGCAGCGACAGTCCAACAGTTCGGGTCTGGAACAAGGCAGTAATGCCGAGGTAT CCTGCTTCCAGCGCGCAAGCCTGCGGGCTCGTTTCGTCGATGCTGATGTGACCATTC CGGCAACAAAGCAGCCAGTTCTGAGTGAAACACATGCGTCTGCAACCAATGTCACTT CTAGAGGGGAGCAAGGAAATGAAAAGGGAAACCTTGACAGCCCAGAGCAAACCACGA AAATAGGAGACGAAGAGAAGGAAGCGAGAACAGACGAGATGGTCGGAGATCCGGAAG AAACACGTGAGAAACATGATCCTCCAACAGTATCACACTTCGAAGACAGAAGTGACC ATAGACAAGTCGATGCCCCAGATTCACTCCCAGAAGCAGCACCTAACGTAGGGAGCC AAAACCCCAATTCAGCAGGAACGCATCCAGACACAAGAGCCACTTCTTCAGTGTCTG TCCCGAGTAACGTCGCTGATGAAGAGGTTGCAGAACGGGTGCCGGCACCTGTTCCGG CGGACCAGTCGTTATCTAGAACTTTACTCCAAAGTGACGAAGCATCTCAACGAAAGA ACCAAACGAAGAGTCTTTCAAAAGCTGAAAGCGTGGACACAGAGGAAATGTCGGCTT TCGTGCTGGACGAAGTCTCTGGGTTCTTTTACGACCAGCAAGGCTACGTGTACGACC AACAAGGAAACCTCAGAGGTTATTTGGATGCCAGTGGAGCTTTCCAGGCGTATTCGG AAAGTGAACTGCAGTATTACGCGGAAACCATGGCAAGAGTTCAAGATCAAGAACAAG CGGACTATGCGTATCCAGAAGGTTAGAGACAAGCTTAGGTATT	Clone TgGT1_233040 catalytic domain (TgPDE15$^{952-1731}$) into pET-*6HIS-SUMO* by HiFi assembly	This work; IDT

927

Separate Supplemental Files

Table S4 IP TgPDE1 TgPDE2 LC-MS/MS.xlsx

Table S5 Crosslinked IP TgPDE1 TgPDE2 LC-MS/MS.xlsx